AALBORG UNIVERSITY

Master Thesis

MOBILE COMMUNICATIONS 2011
Group 11gr1013

A study about the human body influence on the performance of antennas and ways to parameterize this influence

Under the supervision of: Dr. Mauro PELOSI
& Prof. Gert. F. Pedersen

Research conducted by and report written by:

Marc CORNUEJOLS, Guillaume VIGNAL and Arnaud ZEENDER

Abstract

In response to a lack of research in the domain of studies concerning the impact of the human body on the performance of an antenna, this thesis explores this impact. It also tries to determine a criterion concerning the robustness of the antenna with regard of this impact. However it is ultimately shown that their no real criterion, or rather an infinity of them and that the robustness can only be found experimentally.

Acknowledgments

First of all, we would like to thank our supervisor Mauro Pelosi for his guidance and patience. It’s thanks to him and his advices that this thesis reached quality content.

We would like also to thank our second supervisor Gert Frølund Pedersen for his advices and his help.

Finally, we would like to thank Aalborg University and ECE Paris Engineering School for giving us the chance to make our Master thesis in such a prestigious university.

Signatures

Marc Cornuéjols	
Guillaume Vignal	
Arnaud Zeender	

Table of Contents

LIST OF FIGURES

LIST OF TABLES

LIST OF SYMBOLS AND ABREVIATIONS

W_i: The instantaneous Pointing vector

E_i: The instantaneous Electric field

H_i: The instantaneous Magnetic field

P_i: The instantaneous total power

s: A closed surface crossed by the electric and magnetic fields

W_{av}: The average Pointing vector

W_{rad}: The radiated Pointing vector

P_{av}: The average power

P_{rad}: The radiated power

p: The dissipated power

σ: The conductivity

d_k: The defined space step for the FDTD analysis along the axis k

r_{xy}: The correlation coefficient

x_i: The value of the variable x at a given point

y_i: The value of the variable y at a given point

$\bar{x}$: The mean of x

$\bar{y}$: The mean of y

s_x: The sample standard deviation of variables x

s_y : The sample standard deviation of variables y

Γ: The reflection coefficient.

Z_0: The characteristic impedance of the transmission line

Z_A: The impedance at the input of the antenna

Z: The impedance of the antenna

R: The real part of the impedance of the antenna

X: The imaginary part of the impedance of the antenna

FDTD: Finite Difference Time Domain

Epsilon: Permittivity

Sigma: Conductivity

Mu: Permeability

PIFA: Planar Inverted F Antenna

IFA: Inverted F Antenna

INTRODUCTION

Ever since the dawn of wireless communications, antennas have been crucial in the process of designing efficient wireless systems. Being both the transmitting and receiving appendixes of the overall network, their performance has over the years been thoroughly investigated and numerous antenna designs have been thought of and/or implemented.

When considering the case of mobile handset antennas, engineers must face additional challenges, size being the most important of them. To overcome this difficulty, constructors have at their disposal quantity of simulators and a vast number of theoretical or experimental parameters to foresee the overall quality of a design.

Figure 1 User sensitive part of the iPhone 4 antenna [1]

Yet with all these means at their disposal, one of the most important failures still today is the case of the iPhone 4. Why did this unforeseen error happen, and could it have been avoided?

The particularity of the iPhone 4 antenna is that rather than being internal as in many mobile phones, it is actually situated on the outer boundary of the mobile phone. And yet, this design said to be one of the most efficient Apple had ever realized came out to be a near disaster.

The fact is that, as for almost any mobile phone antenna, its design had been thought in free space, and it was most likely tested in experimental free space. This is the reason of the failure of this antenna; it was not considering the impact of the hand when a user was holding the phone.

While this error of implementation could have been avoided via experimentation with actual user body interference, it mainly shows a lack of consideration from mobile phone companies for the said impact. However, this situation has forced manufacturers to deepen their knowledge about user interference and to focus more consequently on this issue.

In this context, the present thesis acts as a study on the impact of the body of the user on antennas and tries to determine a simulation level parameter that could indicate whether or not an antenna is robust to this impact. The main idea around this study being to avoid antenna manufacturers from having to experiment blindly on the topic, benefiting from a trend idea given by the robustness criterion.

As this report is an observation more than a demonstration, there is no hypothesis regarding the reason of the nature of the robustness of an antenna to the human hand impact on its signal.

Before proceeding, here are the detailed limitations taken into account during this research:

- The first limit was that mitigation of the signal by the hand only was considered and not by the head for simplification purposes.
- The second limit was that the iPhone 4 antenna case was not considered (its presence in the title being here to quickly show what type of issue is to be dealt with), this project being solely limited to the definition of a robustness criterion via the use of reference antennas.

The method used to address this topic is twofold. On one hand, it consists of testing antennas with special existing tools, and observing the results that each of these antennas provide when confronted to the proximity of a hand. On the other hand, it consists of analyzing these results to deduct a robustness criterion. The organization of contents follows:

Firstly, the tools of measurement investigated and used are described, followed by other leads the research has required but which had only intermediate or little impact on the choice of a robustness parameter.

Experiments prior to the establishment of these tools and complementary to them are also developed in this part.

Secondly, the FDTD method is described and the software used for the experimentations showed in this report is discussed.

Thirdly, reference antennas are described and analyzed through all the tools previously established and mentionned in the previous section. They are then all compared and ranked by robustness with regard of the human hand interference.

Fourthly, the choice of theoretical robustness criterion and how this choice has come to be is described.

For now, let us focus on the tools used to consider robustness.

CHAPTER ONE: TOOLS OF MEASUREMENT AND SIMULATION

I – Introduction

In order to witness the impact of the hand and the quality of the robustness of an antenna considering this impact, several tools of measurement were required. These tools, pre-existing in AAU3 (the FDTD software used for simulation purposes) or simple fundamental parameters of antennas used in telecoms (S11 parameter, etc), were used as many "lenses" under which each antenna would be observed.

As for the simulation paradigm, this study used AAU3, the FDTD simulator developed by Aalborg University and which was used by PhD students of Aalborg University experimenting for their Thesis [2]. Around this Matlab program, a set of scripts were developed and were bound for the analysis of the results which will be detailed later on.

Briefly, the Finite Difference Time Domain numerical computation method is a way to approximate electric and magnetic fields in space and time particularly efficient for the type of volumes we were considering. Details and basics about FDTD can be found in references [3] and are developed in the following chapter.

Let us now explore the measurement tools developed and the fundamental parameters of antenna used, by short means of theory and explanation on why they are relevant and how to use the results they produce.

II – Power Dissipation

1) Calculation methods of power dissipation

There are two ways to calculate the dissipated power in a Finite Difference Time Domain simulation. The one used by the AAU3 software is based on calculations of the pointing vector. In this method, we consider the instantaneous pointing vector as:

$$W_i = E_i \times H_i$$

Where E_i is the instantaneous electric field and H_i the instantaneous magnetic field.

It has been shown in [4] that from the instantaneous pointing vector, the instantaneous total power can be achieved thanks to the following formula:

$$P_i = \oiint W_i d_s$$

Where s is a closed surface crossed by the electric and magnetic fields (usually a sphere located in the radiating near field).

In order to achieve the average power density, it has also been shown in [4] that the instantaneous pointing vector can be derived into a sum of a harmonic part and a non harmonic part. So when time averaging, the harmonic part disappears, leaving only the average pointing vector (average power density) as:

$$W_{av} = \frac{1}{2} Re[E \times H^*]$$

Similarly to the instantaneous power equation, the average power can be obtained from this formula, the average power is also the radiated power:

$$P_{rad} = P_{av} = \oiint W_{rad} d_s = \oiint W_{av}\, d_s = \frac{1}{2} \oiint Re[E \times H^*] d_s$$

With P_{av} as the average power, P_{rad} as the radiated power, W_{rad} as the average power radiated density, and s a closed surface. By subtraction of the radiated power from the input power (known at the beginning of the simulation), the dissipated power is obtained.

However, for another set of scripts, another calculation method was used, which is to compute cell-by-cell dissipation using the E-field magnitude and the conductivity of the material considered. This computation obviously works only for FDTD simulations which work on a cell-by-cell basis. The formula for this dissipation is given by the following formula, for one cell:

$$p_i = \frac{1}{2}\sigma_i \, |{E_i}^2|$$

With the following parameters:

- p: the dissipated power by unit of volume (W/m^3)
- σ: the conductivity (S/m)
- E: the E field in one cell (V/m)

For each cell, the power dissipated is given by:

$$P_i = \, p_i d_x d_y d_z$$

With the following parameters:

- P: the dissipated power in one cell
- d_k: the defined space step for the FDTD analysis along the axis k (x, y or z)

The total dissipated power can be calculated by:

$$P = \int_{i=0}^{N} P_i d_i$$

With the following parameters:

- N the number of dissipative cells

The resultant equation is thus:

$$P = \int_{i=0}^{N} \iiint \frac{1}{2}\sigma_i \, |{E_i}^2| \, d_i d_x d_y d_z$$

In the case of a cubic space division, dx dy and dz are similar. This is the case of AAU3, where a FDTD cell has equally sized dimensions along each axes. This method is much more convenient as we can obtain a cell by cell approach to power dissipation. As far as the implementation in a Finite Difference Time Domain simulation is concerned, in our case we transform the E and H fields in spherical coordinates before making any computation. Furthermore, since we only consider a near field simulation, we make use of the near to far field transformation technique.

2) Total power dissipation

By its nature, power dissipation is one of the key aspects to explore in order to determine the robustness of an antenna to the human body. While not really deterministic due to its lack of detailed information, the total power dissipation does give us an indication about how much an antenna is impacted by the presence of a hand in its vicinity.

Therefore, antennas will be compared to the mean of the total power dissipated by all antennas and statistics will be shown at the end of chapter 3. The reference antennas will also be analyzed independently on this value of total power dissipation.

3) Power dissipation along an axis

A way to obtain a closer look at power dissipation in a brick is to look at power dissipation separately along each axis. From this, we can obtain another mean of classification. The most pertinent axis for this study is the "radial" axis intersecting both the antenna and the brick (the x axis). Power dissipation occurring in the two first centimeters along this axis provide information regarding the rate at which the power transmitted by the antenna decreases in the hand. This power dissipation will be measured both as a cell by cell graph and as a regrouped by centimeter graph which provides a greater visibility in terms of relative power dissipation.

The analysis of power dissipation offers two types of information. On one hand, the brute analysis of the power dissipated to input power ratio offers valuable knowledge about how much power is dissipated inside the human hand. On the other hand, the analysis of the power dissipated along the radial axis within the hand offers insight on the trend of dissipation the transmitted power goes through.

III – Three Dimensional Correlations

1) Cross-correlation definition and explanation

Correlation can be defined as a measure of coherence between to variables. This meaning that variations within these variables are measured to grasp how much they behave accordingly. [5]

For one-dimensional variables and since in our case equally sized variable arrays are considered (as the size of the domain is kept a constant), this would mean using Pearson's product-moment equation [6]:

$$r_{xy} = \frac{\sum_{i=1}^{n}(x_i - \bar{x})(y_i - \bar{y})}{(n-1)s_x s_y} = \frac{\sum_{i=1}^{n}(x_i - \bar{x})(y_i - \bar{y})}{\sqrt{\sum_{i=1}^{n}(x_i - \bar{x})^2 \sum_{i=1}^{n}(y_i - \bar{y})^2}},$$

Where x_i represents the value of the variable x at a given point, identically for y. In this equation, $\bar{x}$ represents the mean of x and $\bar{y}$ the mean of y. s_x and s_y are the sample standard deviation of variables x and y.

In our case, however, this formula is not sufficient as we consider that a given variable might also vary in space. Thus creating a need for pattern recognition which is provided by another correlation method: the cross correlation.

Cross-correlation is used in several domains like signal processing or medicine. The idea behind it is to apply a delay to one of the "signals" and comparing it to the other signal. This method of statistics is used to recognize tumors on radio scans of patients, for example.

While this method normally applies to different signals, trying to recognize a smaller one with a bigger one, it also applies for our case as the radiation pattern might vary between two measurements (with and without the brick, for example or in the case of different size of domains). The idea being to measure how much the electromagnetic fields vary accordingly when confronted with a slight change in the environment, the introduction of the human hand.

The idea of three dimension cross correlation can be visualized as this: we have a signal A (the results in free space for the fields of an antenna in three dimensions) in a matrix of size $m \times n \times o$ and a signal B (the result with the addition of a brick nearby the antenna) in a matrix of size $i \times j \times k$. Each cell of the A and B matrixes corresponds to a space-cell of the FDTD computation method whose size depends on the space step chosen.

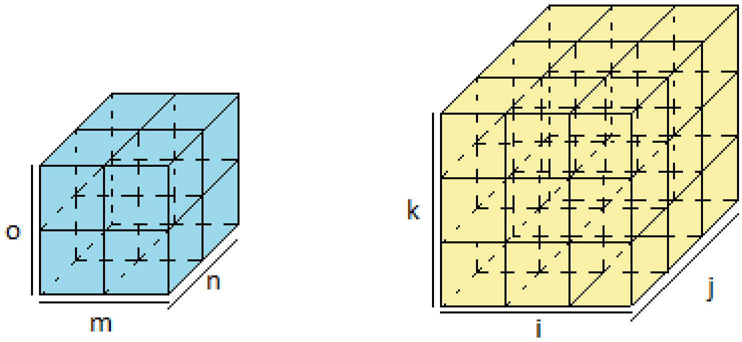

Figure 2 Example sets A and B

The three dimension cross-correlation equation for discrete functions can be, analogously from one dimensional cross correlation, defined as:

$$(A * B)[x, y, z] = \sum_{p=-\infty}^{+\infty} \sum_{q=-\infty}^{+\infty} \sum_{r=-\infty}^{+\infty} A^*[p, q, r] B[p + x, q + y, r + z]$$

This means in fact that the set A will be superimposed over the set B at every possible location and a correlation coefficient will be derived from each of these particular locations. In our case, the result of this is a matrix of dimensions $[m + i - 1, n + j - 1, o + z - 1]$ as all values where A and B do not overlap are of no interest. Figure 3 to Figure 5 illustrate this process.

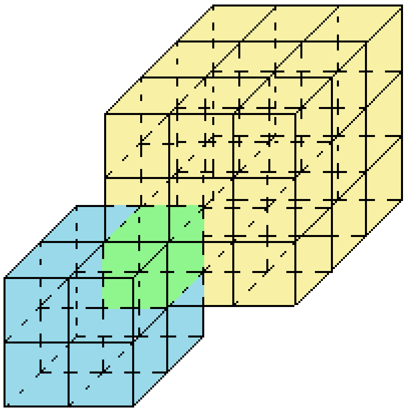

Figure 3 First cross-correlation coefficient computation on overlapping cells

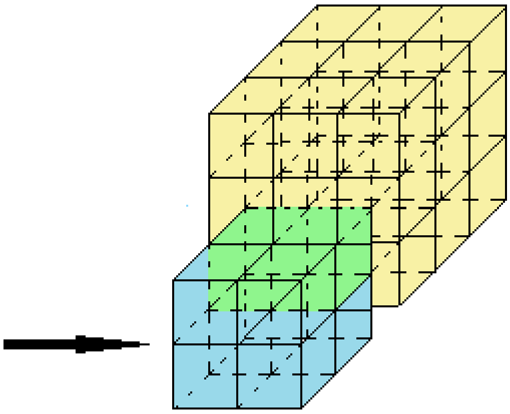

Figure 4 Cross-correlation coefficient computation

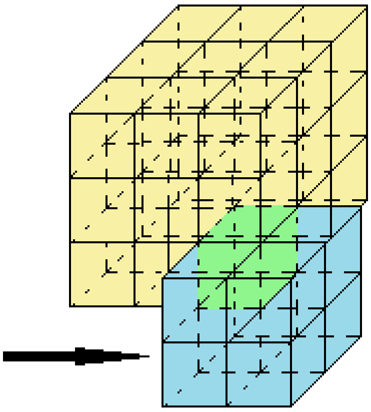

Figure 5 Fourth cross-correlation coefficient computation

Then, by transposition on different rows and columns, all matching possibilities between set A and B are thus explored.

In our case, there are two possible scenarios for the use of correlation. Either as described above we simulate a reference antenna in free space in a small domain then simulate in a wider domain the same antenna with a brick in its vicinity. The aim of the cross-correlation in this case is to find a matching E-field pattern inside the wider domain.

The second possibility is a simpler correlation in the case where the size of the domains in free space and brick simulation are identical. In this case, to refer to Figure 3 to Figure 5, we only consider the correlation coefficient at the exact spot where both variable matrixes perfectly match one another. This second method has given better results and is thus mainly used in the parts below.

2) Interpretation of results

As the correlation calculation results in a correlation coefficient, it is important to know how to interpret it. In the case of different-sized domains and "pattern" recognition, results have shown that very high correlation coefficients are attained when nearly null electromagnetic fields are correlated (on the edges for example, when only part of each set of result overlap).

A correlation coefficient ranks from -1 to +1, depending on the type of relationship correlating the two variables or, in our case, sets:

- A correlation coefficient of +1 indicates a positive relationship, meaning that when one variable increases or decreases, so does the other one.
- A correlation coefficient of -1 indicates a negative or opposite relationship, meaning that one set of data behaves oppositely to the other.
- A correlation coefficient of 0 means that there is no link between the two variables.
- In a general manner, if the absolute value of the correlation coefficient is above 0.7 it is considered as a high correlation between the variables, on the other hand absolute values lower than 0.3 indicate a low correlation.

However, correlation does not indicate causality. In our case, this means that even if an antenna has a very high correlation coefficient between free space and brick simulations, it does not mean that it is linked to the free space simulation. It might however mean that the resistance to the brick is higher for this antenna. The 3-D correlation is used as a measurement of how much the fields are affected by the presence of the brick and more importantly how much these fields are predictably affected.

Let us now proceed to another tool of measurement, the S11 parameter analysis.

IV – S11 Parameter

To understand the concept of the S11 parameter, let us consider a transmission line represented by a two-port network where on one end lays the source and on the other the antenna itself (Figure 6).

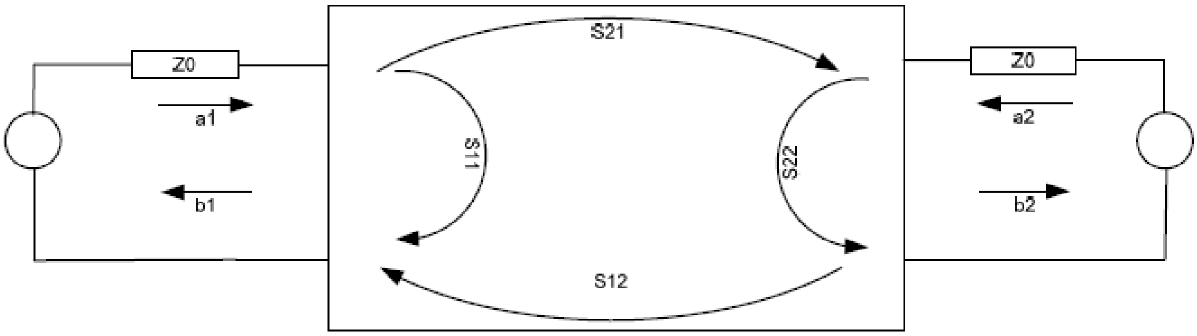

Figure 6 A two port network representing a transmission line [10]

The concept of the S11 parameter is simply to represent the reflection coefficient at the input of the transmission line. The value of this parameter should be the lowest possible at the resonance frequency of the antenna. Ideally, this would mean a value of 0 but in that a -10dB is often considered as sufficient [7].

The formula for the reflection coefficient is given by:

$$\Gamma = \frac{Z_0 - Z_A}{Z_0 + Z_A}$$

Where Z_0 represents the impedance of the transmission line and Z_A represents the impedance at the input of the antenna. To get a perfect matching (a reflection coefficient with a value of 0), we need to have an identical value for Z_A and Z_0.

The reflection coefficient varies with frequency and can thus have a plot which looks like the one in Figure 7.

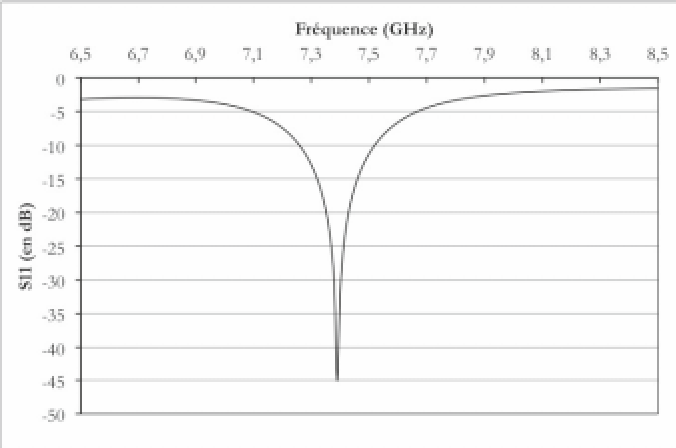

Figure 7 A S11 plot as a function of frequency

From this graph much information is obtained. First, it is possible to compute the bandwidth by looking at the -6dB values (though several bandwidth are available, only the -6dB bandwidth is considered). In Figure 7, for example, the bandwidth is about 0.55 GHz. Secondly, it is also possible to get the resonant frequency where the S11 parameter is at the lowest, which in the graph would be around 7.4 GHz.

The S11 graph is a key tool to see the impact of the hand on an antenna. Indeed it is a key tool to observe the impact on the bandwidth, but also on the effect on the resonant frequency and “depth” of the S11 parameter.

Let us now focus on experiments achieved prior to the robustness experiment with the aim of expanding our knowledge on specific topics related to the robustness experiment.

CHAPTER TWO: SIDE EXPERIMENTS

Aside from the main experiment about the determination of a robustness criterion, this research has pushed into several sub-areas related to the topic, based on references read to understand the topic or simply to determine as accurately as possible the way the tools described above would be used.

I – Conductivity, permittivity and permeability variations

As this project is about the effect of the human body on the performance of antennas, it is important to study the properties of the human body, and more specifically, the hand.

The human hand is composed of several layers (fat, skin, bone, flesh et cetera) which have distinct values for conductivity (the ability to conduct current), permittivity (the measure of resistance to electric field formation) and permeability (the degree of magnetization of a material in response to a magnetic field).

However, the impact of these parameters on power dissipation within a brick is unknown. The purpose of this experiment is to determine the impact of the variation of these three parameters on the power dissipation of the electric fields.

From the definition of these parameters, the hypothesis for this experiment is that the greater the conductivity is, the more power will be dissipated (as shown in the part Power Dissipation above). Likewise, permittivity should increase power dissipation and permeability should decrease it. Also, past a certain value, dissipation should stabilize to a maximum.

In order to conduct this experiment, a PIFA antenna resonating at 1GHz is considered to be facing a brick of 40x250x250 millimeters at the distance of 30 millimeters from the antenna. The rest of the medium is considered to be free space. The values of conductivity, permittivity and permeability are modified one by one in order to witness an un-biased impact of these variations. This experiment is conducted using AAU3. As for results, power dissipation along the radial axis is considered. Figure 8 below shows the layout of the experiment.

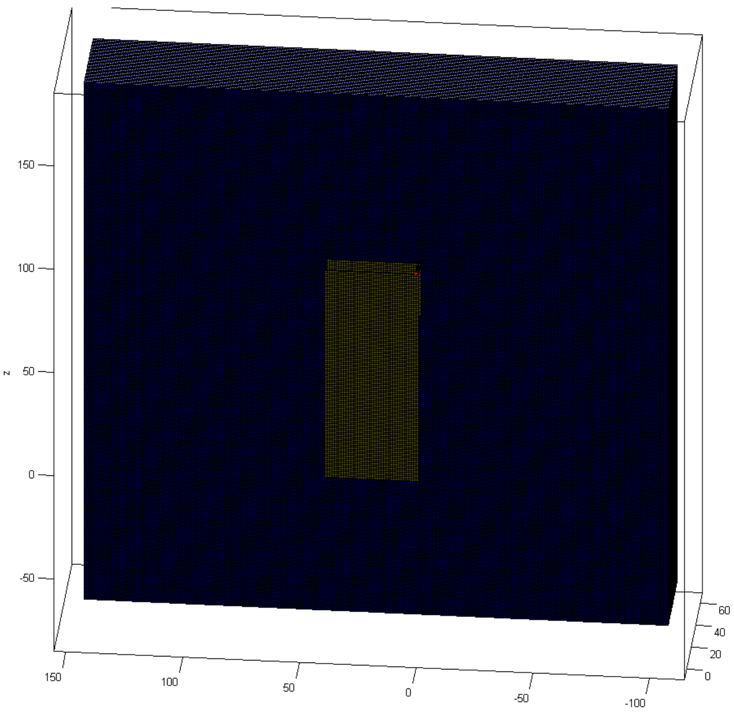

Figure 8 Scheme of the variations experiment, a PIFA antenna facing a brick

In Table 1 and figures below, the results of this experiment are compiled.

Sigma	Mu	Epsilon	Pdis C by C	Pdis < 3cm	% of total
0,85	1	42,5	8,34E-10	7,10E-10	85,11
1	1	42,5	8,52E-10	7,47E-10	87,68
2	1	42,5	8,05E-10	7,79E-10	96,75
3	1	42,5	7,11E-10	7,04E-10	98,92
4	1	42,5	6,34E-10	6,30E-10	99,44
1	1	1	1,04E-09	1,02E-09	97,80
1	1	1,5	1,05E-09	1,03E-09	97,71
1	1	2	1,06E-09	1,03E-09	97,61
1	1	10	1,11E-09	1,06E-09	95,65
1	1	20	1,05E-09	9,74E-10	92,71
1	1	30	9,04E-10	8,13E-10	90,00
1	2	42,5	1,10E-09	1,02E-09	93,05
1	4	42,5	1,48E-09	1,43E-09	96,74

Table 1 Results of the variations experiment

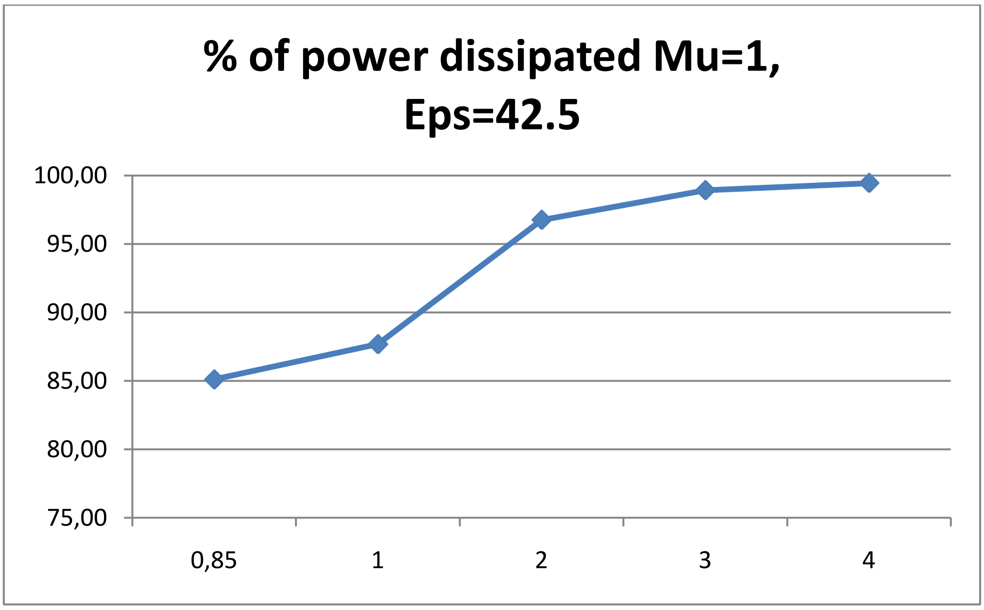

Figure 9 Relative power dissipation according to the variation of sigma

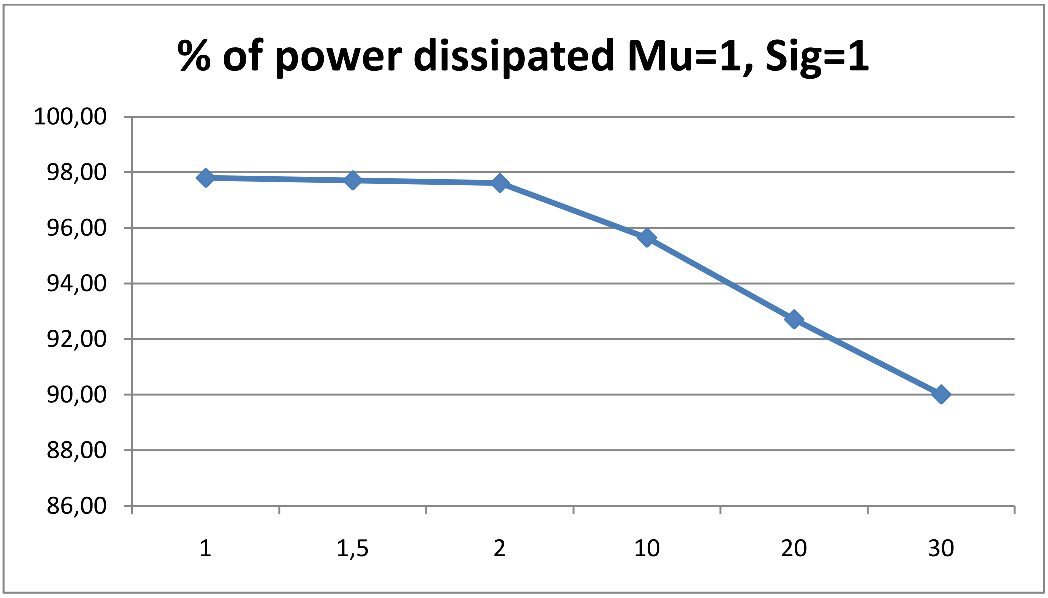

Figure 10 Relative power dissipation according to the variations of epsilon

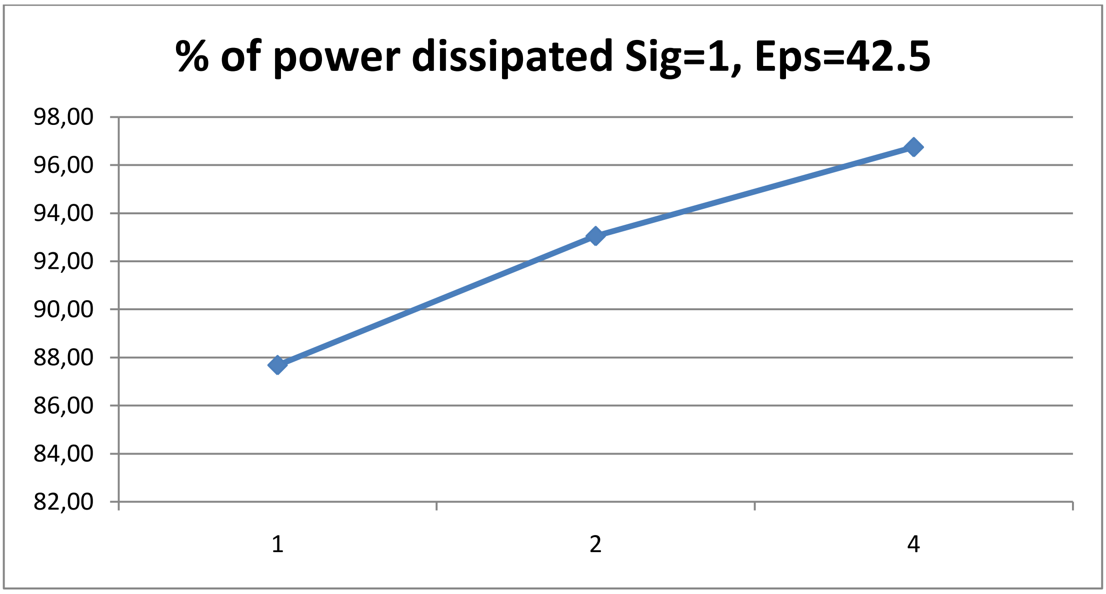

Figure 11 Relative power dissipation according to the variation of mu

These results can be interpreted as such:

- From Figure 9 and Table 1, it can be seen that an increased value of conductivity decreases the cell by cell power dissipation from 8.52×10^{-10} to 6.34×10^{-10} almost linearly. However, increasing the conductivity also increases the percentage of the total power dissipated in the first three centimeters as we can see in Figure 9. The percentage of the total power dissipated in the first three centimeters increases linearly with the increase of the conductivity to reach a maximum of almost 100% when the conductivity is near 3 S/M.

- From Figure 10, it can be seen that increasing the permittivity (epsilon) increases the total power dissipated pseudo-linearly from $1.04x10^{-10}$ to a maximum of $1.11x10^{-10}$ when epsilon reaches 10. When epsilon is greater than 10, the total power dissipated decreases linearly. Also, increasing the permittivity linearly decreases the power dissipated in the first three, from 98% to 90% in Figure 10.
- From Figure 11 and Table 1, it can be seen that increasing the permeability (mu) increases the total power dissipated in a logarithmic manner from $8.52x10^{-10}$ to $1.48x10^{-9}$. In the same manner, increasing the permeability of the brick logarithmically increases the power dissipated in the first three centimeters (Figure 11), from 88% to 97%.

In the same manner, some results have shown that the repartition of power dissipation varies a great deal when varying parameters as shown in Figure 12 and Figure 13 below.

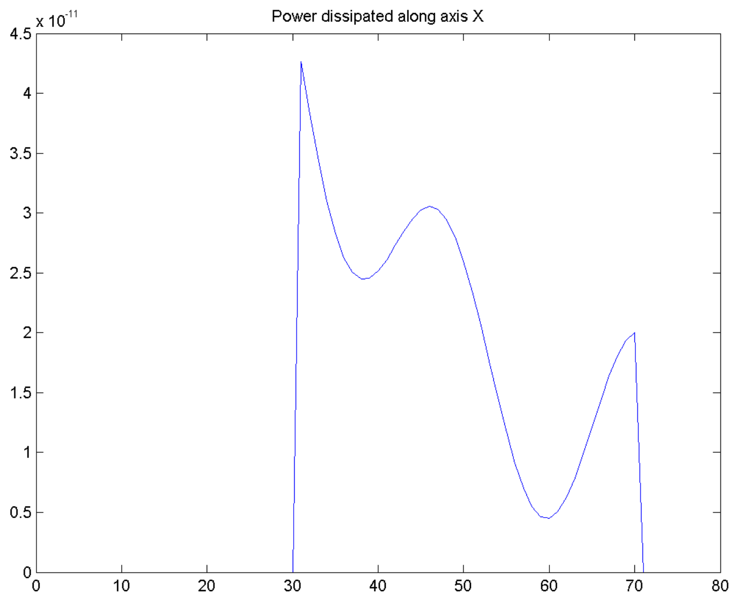

Figure 12 Power dissipation (in W) along the x-axis with a permeability of 42.5

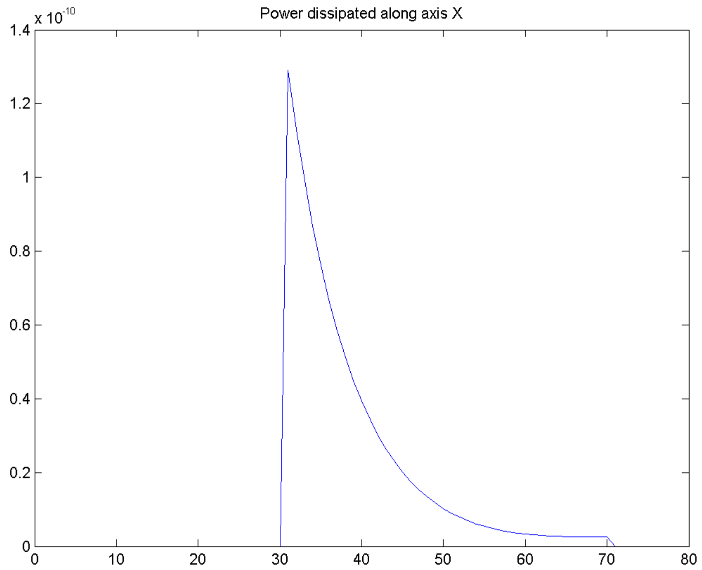

Figure 13 Power dissipation (in W) along the x-axis with a permeability of 1.5

From Figure 12 and Figure 13, it can be seen that the repartition of the power dissipation within the brick varies with the change of permeability. While this variation cannot be measured in terms of metrics, it can be graphically observed in the figures above. A low permeability (1.5 V*s/(A*m)) provokes a sharp decrease of power dissipation after the first millimeters. However, a higher permeability (42.5 V*s/(m*A)) makes the power dissipation within the brick more chaotic, with three separate peaks in power dissipation along the radial axis.

The variation of total power dissipation with regard of variations of conductivity, permittivity and permeability can be metrically measured and follow the definition of these parameters. However, the impact of these variations on the localization of the power dissipation within the brick is less measurable. Indeed, peaks of power dissipation may appear with the variation of one parameter (like the permeability as shown above).

With this in mind, simplifications for the hand were taken from the literature [14] and for the remainder of the project, the hand will be considered as having parameters of permittivity (mu) =1, conductivity (sigma) =0.79 S/m and permeability (epsilon) = 36.2 V*s/(m*A).

II – Narrowband PIFA study

One of the antennas present in this survey is the narrowband planar inverted-F antenna (Narrowband PIFA). It is a particular case of the PIFA antenna where the PIFA is set close to the ground plane.

However, the link between the distance of the antenna from the ground plane and the depth of the S11 parameter and bandwidth was unclear. This experiment has for objective to show this link.

The hypothesis of this experiment is derived from literature [4], which states that the closer an antenna is brought to the ground plane, the smaller the bandwidth and the reflection coefficient are.

In this experiment, we consider a Narrowband PIFA set to function in the UMTS V standard (850 MHz). The already available reference PIFA antenna was separated from the ground plane by 10 millimeters and this study used values of 1, 2 and 5 millimeters between the ground plane and the antenna to witness the impact of this distance on the reflection coefficient. The layout of this experiment can be seen in Figure 14.

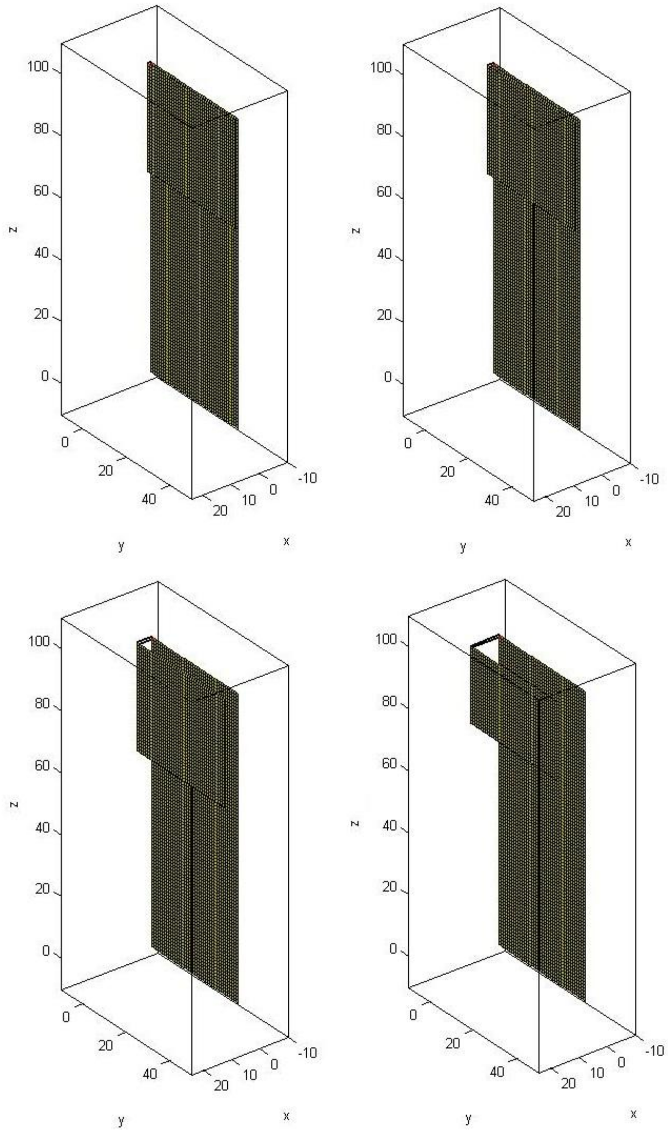

Figure 14 PIFA antennas separated by 1, 2, 5 and 10mm from the ground plane

The results obtained from this experiment, are shown in Figure 15 and further expanded in Table 2 below.

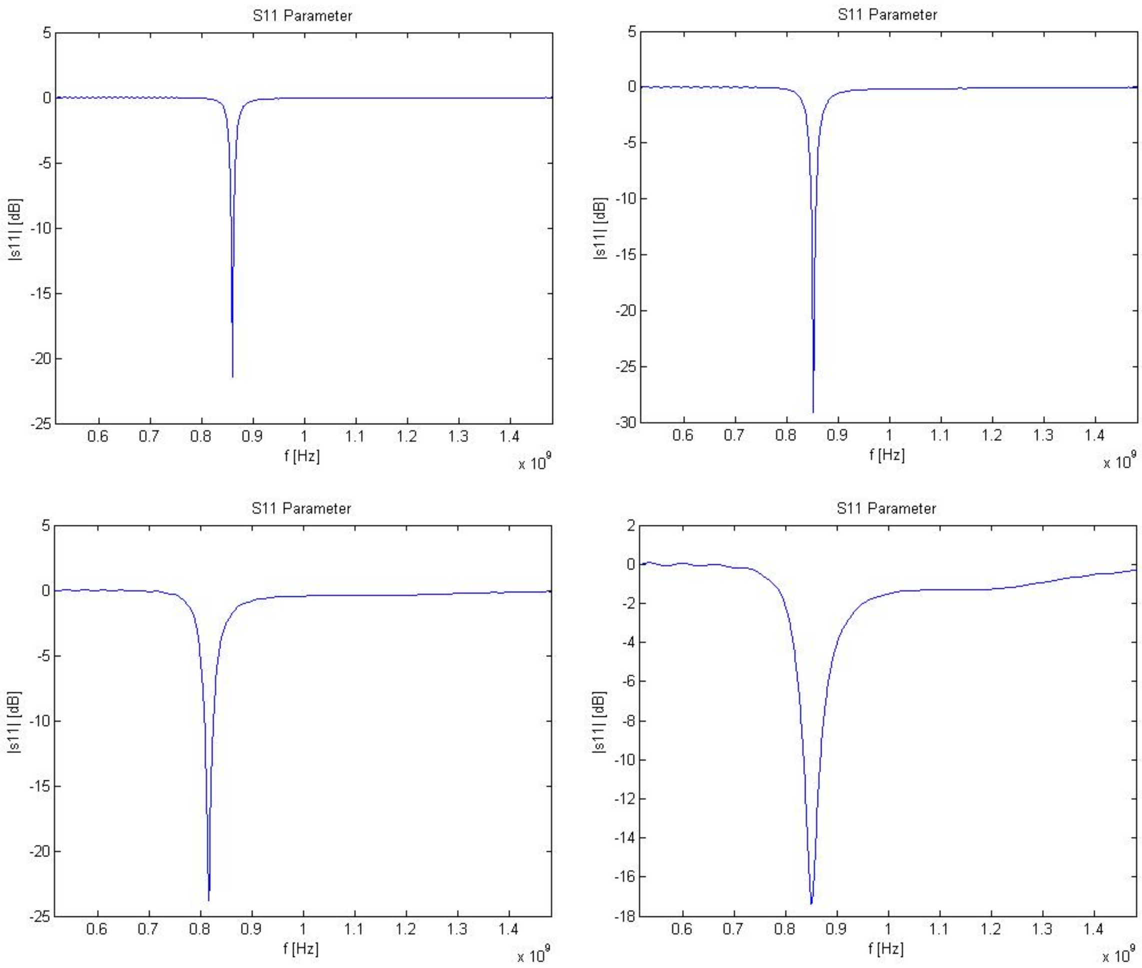

Figure 15 Reflection coefficient for PIFA antennas elevated by 1, 2, 5 and 10mm

From Figure 15 above, numerical results are compiled in Table 2 below.

Distance from Ground plane	Bandwidth	Reflection coefficient
1	10 MHz	-22 dB
2	20 MHz	-29 dB
5	35 MHz	-24 dB
10	80 MHz	-17 dB

Table 2 Impact of distance from the ground plane on PIFA antenna performance

The general trend that can be observed from these results is that with elevation, the bandwidth of the antenna increases, but its reflection coefficient increases as well, making the antenna more vulnerable to interference. The hypothesis is verified.

This experiment gives a clear insight on the impact of the distance set between the antenna and the ground plane. The height used for the antenna determines the bandwidth of the antenna and the value of the reflection coefficient. This experiment has allowed the reference narrowband PIFA antenna used later in this report, for the robustness experiment. This narrowband PIFA antenna is set 1 millimeter away from the ground plane as it offers much variation from the 10 millimeter case and will thus be much more relevant when considering robustness variations.

III – Impact of the permittivity of the substrate on a thin substrate-layered PIFA antenna

One of the reference antennas considered for the robustness experiment was a thin layered substrate PIFA antenna. From the content available in literature [7], it was clear that the role of the permittivity of the substrate plays a role in the bandwidth of the antenna.

However, there was little content on the measurement of the impact of permittivity of the substrate. As the thin-layered substrate antenna was one of the reference antennas for this survey, it was chosen to investigate further this topic.

From the literature, the hypothesis is that with the increase of the permittivity, the bandwidth and the reflection coefficient will decrease. The resonant frequency should not vary.

In order to run this experiment, a PIFA antenna resonating at 850MHz was used, and a thin layer of substrate (1mm) was placed next to the resonating component of the antenna. The permittivity of the substrate was set to specific values and the reflection coefficient was duly analyzed. Figure 16 represents the layout of the experiment.

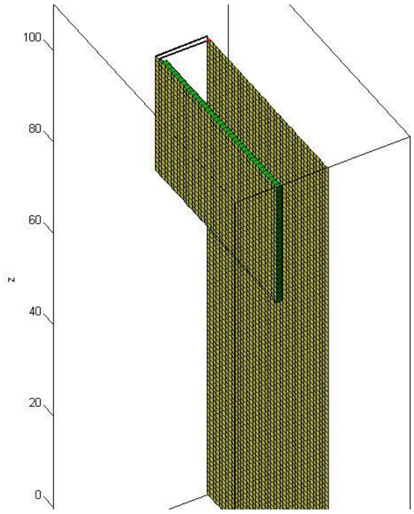

Figure 16 Thin-layered substrate PIFA antenna

The considered values of permittivity were 1, 2, 2.3, 2.5, 2.7 and 3 F/m. Results of this experiment are shown in Figure 17 below and expanded in Table 3.

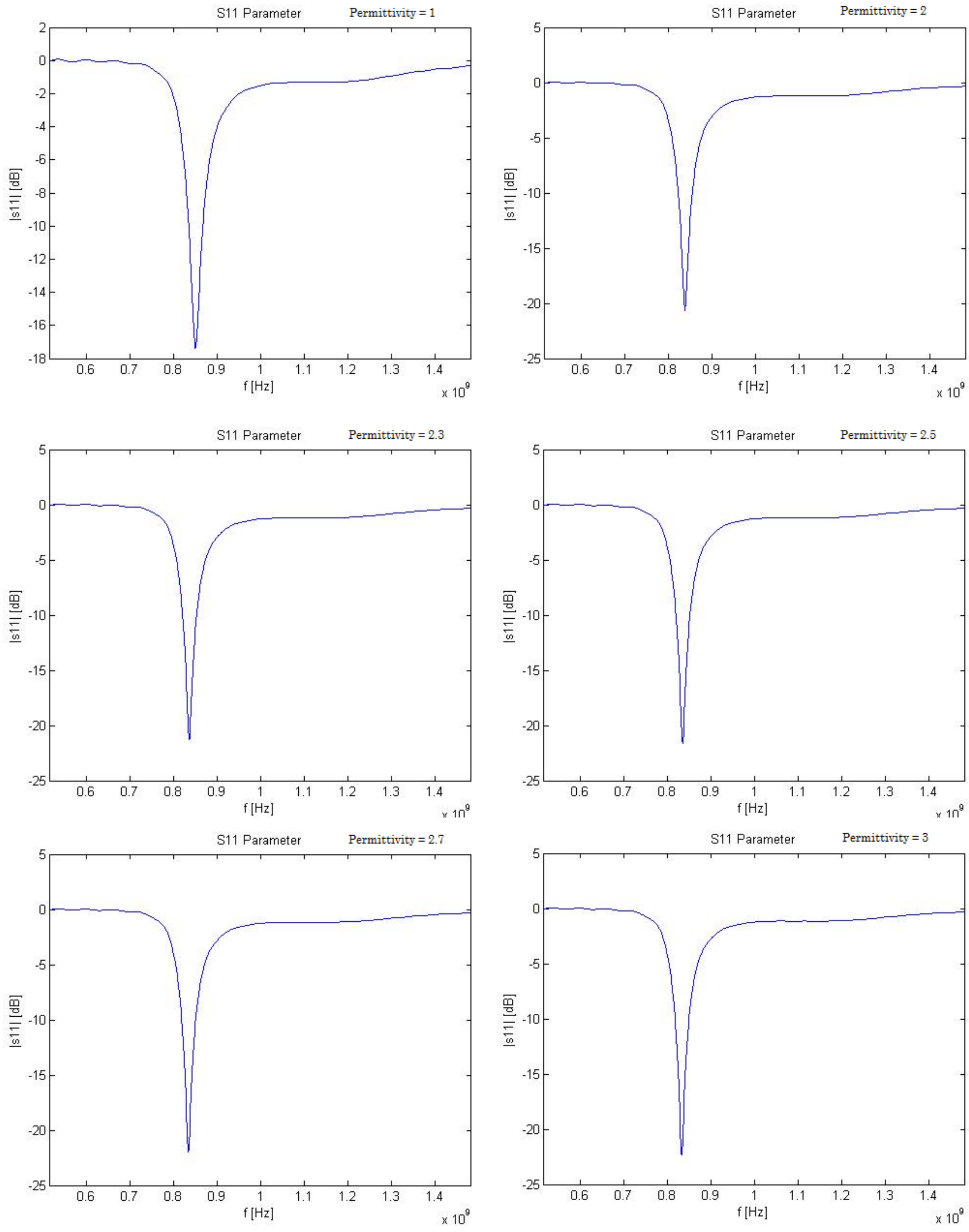

Figure 17 Performance variation for substrate PIFA antennas with different permittivity for the substrate

Permittivity	Resonance frequency	Bandwidth	Reflection coefficient
1	850 MHz	60 MHz	-17 dB
2	830 MHz	50 MHz	-20 dB
2.3	830 MHz	40 MHz	-22 dB
2.5	830 MHz	35 MHz	-23 dB
2.7	830 MHz	30 MHz	-23 dB
3	830 MHz	25 MHz	-23 dB

Table 3 Performance variation of a thin-layered substrate PIFA antenna with a change of permittivity of the substrate

From the results shown in Figure 17 and compiled in Table 3, it can be seen that when the permittivity increases, the bandwidth decreases. The decrease of bandwidth has an exponential behavior. This coincides with the material available in the literature and the hypothesis. However, the reflection coefficient, if it does decrease at first, it then stabilizes at the value of -23dB. This opposes the basic hypothesis. As for the frequency, it seems immobile except for one value of the permittivity (1 F/m).

The conclusion of this study is that when increasing the permittivity of the substrate, the reflection coefficient decreases to a minimum (in our case of -23 dB), the resonance frequency varies little and more importantly, the bandwidth decreases with the increase of permittivity. With this knowledge in mind, and this robustness survey needing mostly large band antenna, it was chosen that a reference thin-layered substrate PIFA antenna would be used for the robustness simulations.

IV – Defining the composition of the human hand

One of the key features for this survey is to offer a brick with human-hand like behavior regarding the impact on antenna performance. Several studies have shown the impact of different hand considerations on the dissipation of the signal going through the hand.

In order to determine the best brick to test our antennas, it was decided to reproduce some experiments from an article published in Microwave and optical technology letters [15], dealing with the different impact of the bone, skin, fat, blood, etc. on the power dissipation within the hand. The goal of this experiment was to compare those results with the ones obtained using the AAU3 software. That way, the results obtained by the robustness experiment below could prove to be coherent with the ones obtained in Reference [15].

As this experiment is about replication, there is no hypothesis other than that of expecting to find identical results than the reference paper.

The experiment as described in Reference [15] used a dipole facing two successive layers of varying characteristics. In order to proceed in AAU3, two consecutive bricks of width of 7mm and 8mm were implemented 5mm next to a dipole resonating at 900MHz. These bricks have the same width as in the reference experiment. However, they are not infinite in length and height. Figure 18 shows the layout of the experiment. The characteristics of the bricks are identical to the ones available in the original experiment and are taken between the following components:

Material	permittivity	conductivity
Tissue-Equivalent Liquid (TEL)	42.50	0.850
Muscle	55.95	0.969
Bone	16.62	0.242
Fat	5.00	0.025

Table 4 Values of specific hand components

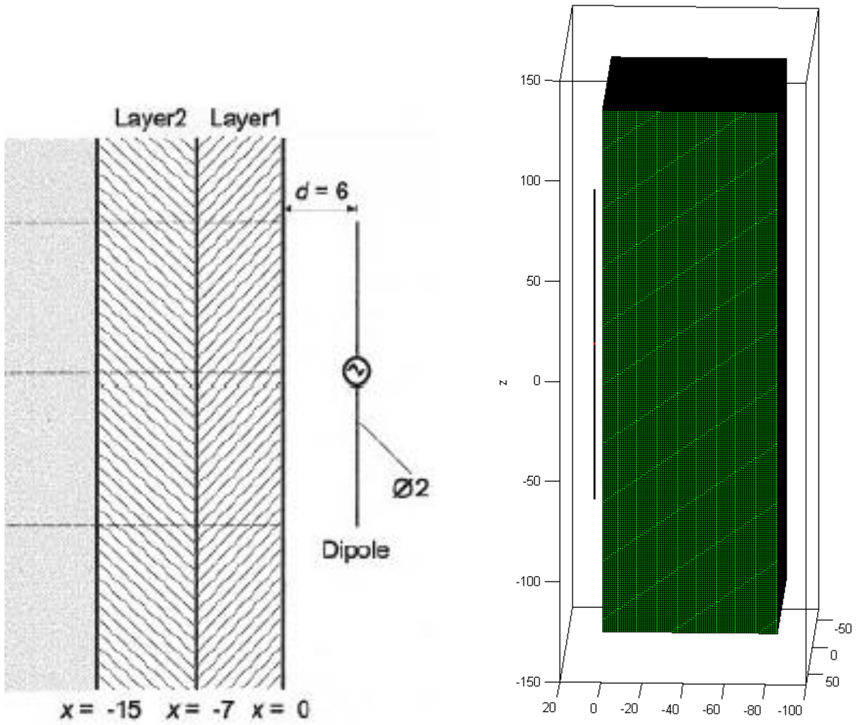

Figure 18 Comparative experiments

Three configurations were studied:

1. The 1st layer represents a fat layer, the 2nd layer represents a Tissue-Equivalent Liquid (TEL)
2. The 1st layer represents a muscle, the 2nd layer represents a bone
3. The 1st layer and the 2nd layer represent a TEL

In every case, after the 2nd layer, we have added a TEL layer that covers the remaining space (from -15mm to -80mm).

The results obtained from AAU3 have been exported and then used in a custom Matlab script to have a resulting display as close as possible to the paper one.

These results are shown on the following figures.

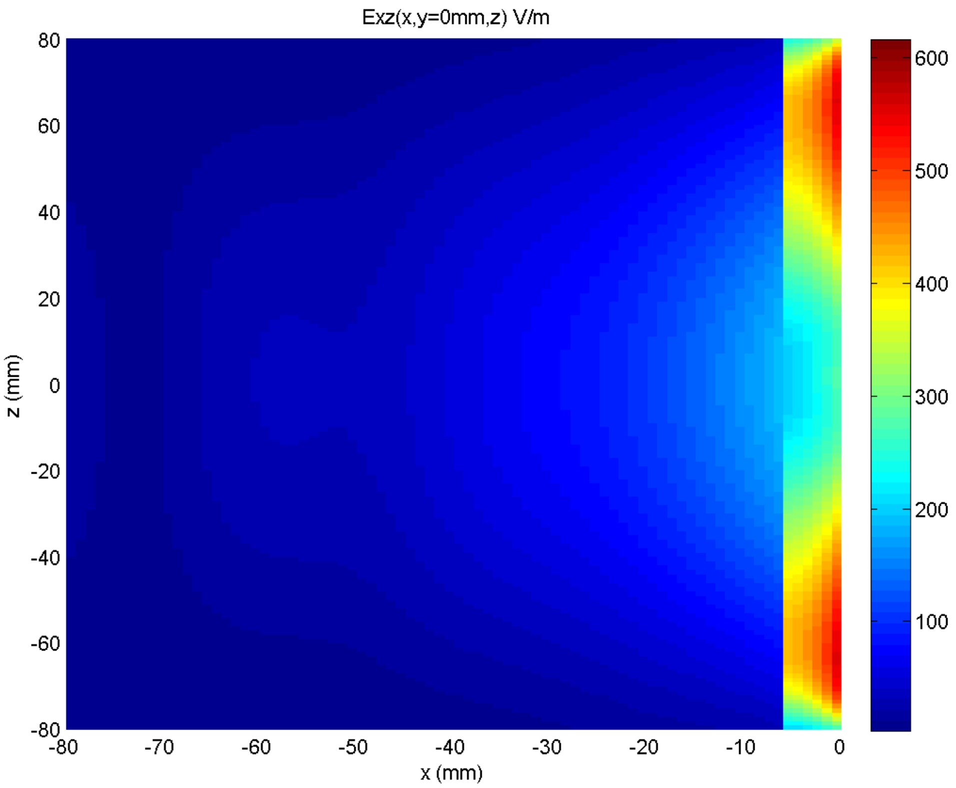

Figure 19 TEL + Fat – Experimental result

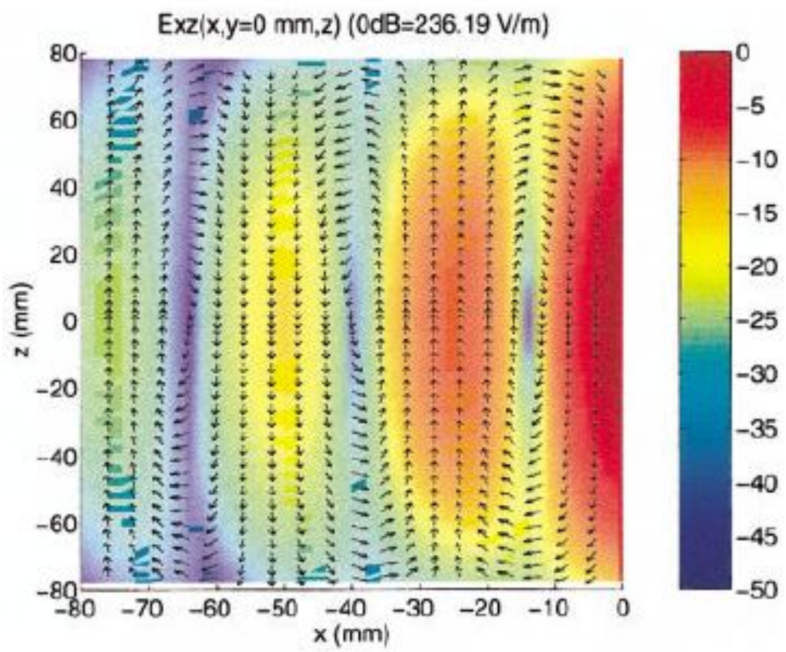

Figure 20 TEL + Fat – Paper result

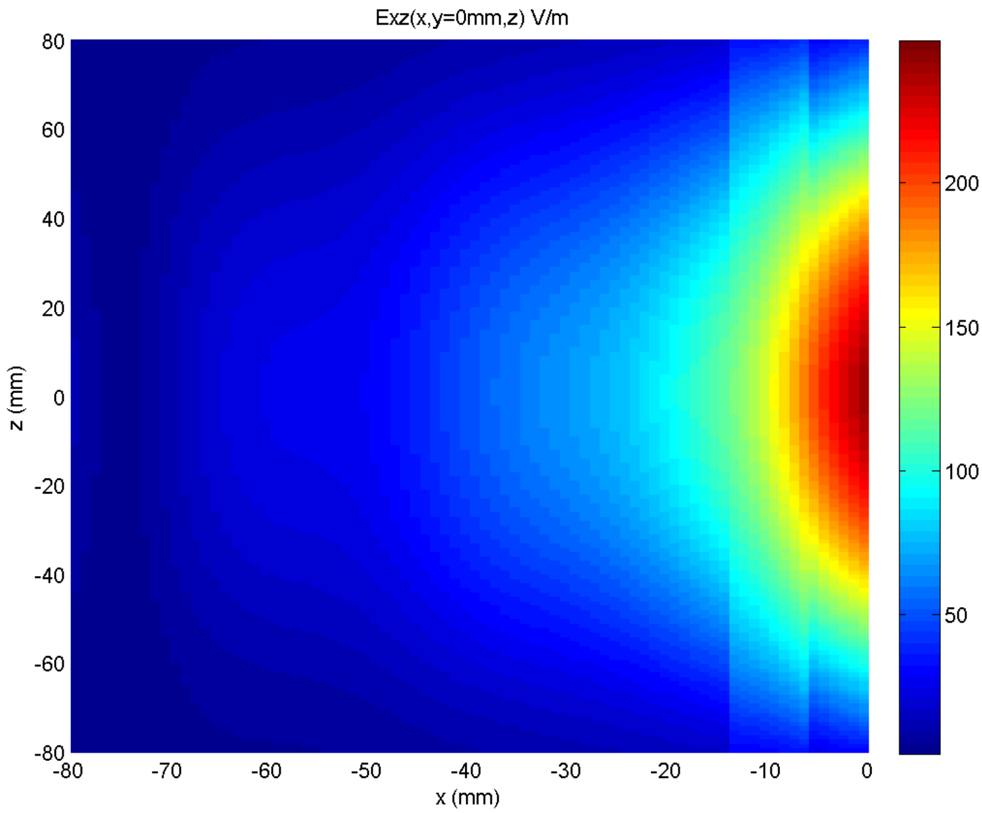

Figure 21 TEL + Bone + Muscle – Experimental result

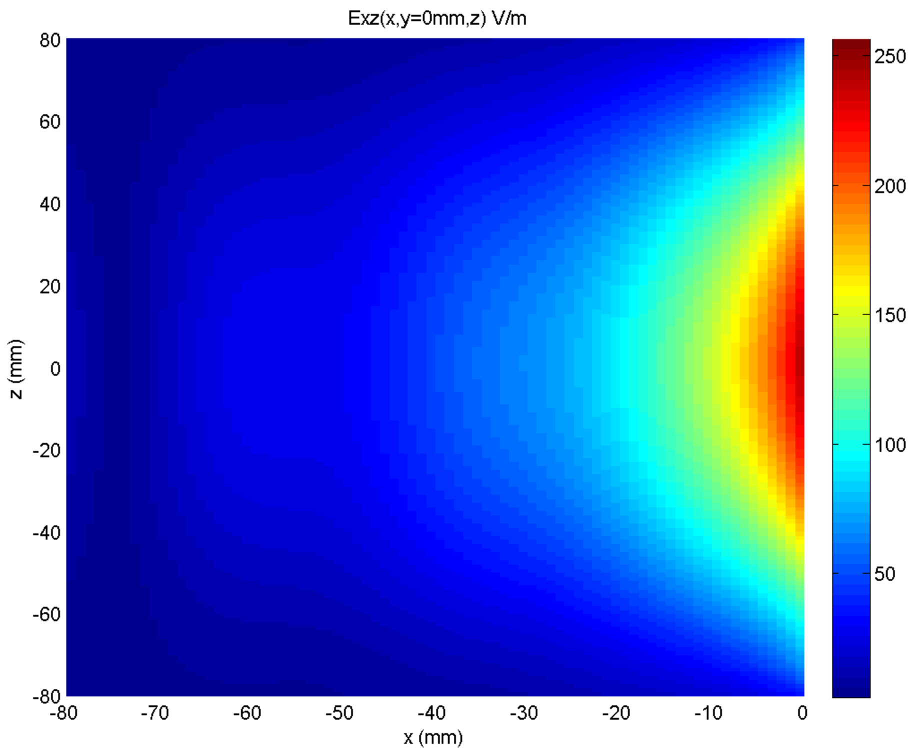

Figure 22 TEL – Experimental result

While results are comparatively similar to those in the article [15], the graphic interface for the results used in AAU3 was not precise enough to obtain the level of details obtained in the article [15].

The following table is presenting a sum up of the results obtained from our simulations.

Tissue layers	Max. E_{xz} (V/m) (y= 0)	Max. E_{xz} Coordinates (mm)	Max. E_{xy} (V/m) (z fixed)	Max. E_{xy} Coordinates (mm)
TEL	237.9	(-1, 0, 0)	0.6397	(-1, 0, 0)
TEL + bone + muscle	240.3	(-1, 0, 0)	0.4279	(-1, 0, 0)
TEL + fat	546	(-1, 0, -67)	543,7	(-1, 0, -67)

Table 5 Maximum E-field Values and Their Positions (values are normalized to 1W input power)

Much like the article, the conclusion of this experiment is that depending on the consideration of the components of the human hand, the points of maximum power dissipation might not be where theory would say. However, in the case of the robustness experiment conducted in this paper, the interesting factor is the observation of the way power dissipation operates in volumes. Furthermore, the similarity of results obtained both by the article and the AAU3 software credits the results obtained by this experiment as authentic.

CHAPTER THREE: SIMULATION PARADIGM AND ALTERATION

I – Introduction

As described in the introduction, we used for this project a Finite Difference Time Domain approach to the computation of fields near our antennas. This FDTD analysis was made possible via the AAU3 software, a Matlab based software allowing us to design antennas and simulate their theoretical fields and such in a very customizable manner [16]. Furthermore, this software allowed us to design objects with specific parameters (like the hand or just a brick) to be put close to the antenna.

During this project, the Aalborg University super computer Fyrkat was used, offering tremendous reduction in computation time of the FDTD method.

First, a general approach to the theory behind FDTD will be given. Then, the process of finding the appropriate brick will be discussed and finally some code alterations will be discussed.

II – An overview of FDTD

1) Introduction to FDTD

With the rise of capabilities offered by new technologies over the past fifty years, simulation capabilities have drastically improved. While frequency-domain solutions were almost impossible to implement with mechanical calculators, there use has been popularized with the appearance of micro-processors. Of these frequency-domain computation techniques, two have mainly emerged: high-frequency asymptotic methods [3] and integral equations. However both these techniques have drawbacks, and the Finite Difference Time Domain (FDTD) method solves some of them. The high-frequency asymptotic method does not perform well on the analysis of non metallic material and the integral equation method, being a linear equation system solving method, potentially requires huge amounts of computer resources to perform correctly.

These limitations have drawn attention to the time-domain solution, and FDTD being the first among them has remained the subject of much development over the past decades. The key benefits of FDTD are:

- FDTD does not use linear algebra, which limits the number of unknown fields as the processor has bounded resources.
- FDTD is robust and accurate; the limits of this method are known and can be avoided, as described below.
- FDTD is an expanding topic of research.

Let us now discuss the principles of FDTD, its limitations and how to avoid them.

2) The principle of FDTD

FDTD is a space-grid computational method designed to solve Maxwell's equations. As such it is based on volumetric sampling of unknown electric and magnetic fields in space. The space lattice, or sampling, is generally equal to one tenth or one twentieth of the characteristic wavelength at which the system is analyzed. Finite Difference Time Domain is, as its name implies, a time domain method. The unknown fields are computed with regard to a specific time and space. The space lattice has been described below; the time step will be discussed later as it is a matter of numerical stability of the system at-hand.

FDTD is "marching in time procedure" [3], this means that fields are calculated from time step to time step, and each computation at a given point in time refers to previous time step computations. As such it is a recursive computation method.

From reference [3], the idea of FDTD is understood by its one-dimensional case then extended to three dimensions. It can be shown that a one dimension scalar wave equation can be derived from Maxwell's (curl) equations. This one-dimensional wave equation is:

$$\frac{d^2u(x,t)}{dt^2} = c^2 \frac{d^2u(x,t)}{dx^2}$$

Where u can be either a direction component electric field E (V/m) or of magnetic field H (A/m). This equation constitutes the basic brick of FDTD which the method solves thanks to the Taylor series expansion:

$$f(x) = f(\hat{x}) + f'(\hat{x}) \cdot (x - \hat{x}) + \frac{f''(\hat{x})}{2!} \cdot (x - \hat{x})^2 + \frac{f'''(\hat{x})}{3!} \cdot (x - \hat{x})^3 + \dots$$

Considering two shifts of u in order to retrieve the second order derivatives, this expansion can be applied to u:

$$u(x_i + \Delta x)\big|_{t_n} = u\big|_{x_i,t_n} + \Delta x . \frac{\partial u}{\partial x}\bigg|_{x_i,t_n} + \frac{\Delta x^2}{2} . \frac{\partial^2 u}{\partial x^2}\bigg|_{x_i,t_n} + \frac{\Delta x^3}{6} . \frac{\partial^3 u}{\partial x^3}\bigg|_{x_i,t_n} + \frac{\Delta x^4}{24} . \frac{\partial^4 u}{\partial x^4}\bigg|_{\xi_1,t_n}$$

$$u(x_i - \Delta x)\big|_{t_n} = u\big|_{x_i,t_n} - \Delta x . \frac{\partial u}{\partial x}\bigg|_{x_i,t_n} + \frac{\Delta x^2}{2} . \frac{\partial^2 u}{\partial x^2}\bigg|_{x_i,t_n} - \frac{\Delta x^3}{6} . \frac{\partial^3 u}{\partial x^3}\bigg|_{x_i,t_n} + \frac{\Delta x^4}{24} . \frac{\partial^4 u}{\partial x^4}\bigg|_{\xi_2,t_n}$$

Where ξ_1 is a point located in the interval $(x_i, x_i + \Delta_x)$, and ξ_2 is a point located in the interval $(x_i - \Delta_x, x_i)$. By adding these two equations, the following equation is obtained:

$$u(x_i + \Delta x)\big|_{t_n} + u(x_i - \Delta x)\big|_{t_n} = 2\,u\big|_{x_i,t_n} + \Delta x^2 . \frac{\partial^2 u}{\partial x^2}\bigg|_{x_i,t_n} + \frac{\Delta x^4}{12} . \frac{\partial^4 u}{\partial x^4}\bigg|_{\xi_3,t_n}$$

Where ξ_3 is a point located in the interval $(x_i - \Delta_x, x_i + \Delta_x)$. By rearranging this equation, the following is obtained:

$$\frac{\partial^2 u}{\partial x^2}\bigg|_{x_i,t_n} = \left[\frac{u(x_i + \Delta x) - 2u(x_i) + u(x_i - \Delta x)}{(\Delta x)^2}\right]_{t_n} + O\left[(\Delta x)^2\right]$$

Where $O[(\Delta_x)]$ is a shorthand notation for the remainder term. From there, a shorthand notation of this equation can be written as follows:

$$\frac{\partial^2 u}{\partial x^2}\bigg|_{x_i,t_n} = \frac{u^n{}_{i+1} - 2u_i^n + u^n{}_{i-1}}{(\Delta x)^2} + O\left[(\Delta x)^2\right]$$

Where u_i^n means $u(i\Delta_x, n\Delta_t)$. This procedure is analogous for the second order time derivative. Both second order derivatives can be inserted into the wave equation, giving:

$$\frac{u_i^{n+1} - 2u_i^n + u_i^{n-1}}{(\Delta t)^2} + O\left[(\Delta t)^2\right] = c^2\left(\frac{u_{i+1}^n - 2u_i^n + u_{i-1}^n}{\Delta x^2} + O\left[(\Delta x)^2\right]\right)$$

By rearranging, this equation transforms into:

$$u_i^{n+1} = \left(\frac{c\Delta t}{\Delta x}\right)^2\left[u^n{}_{i+1} - 2u_i^n + u^n{}_{i-1}\right] + 2u_i^n - u_i^{n-1} + O\left[(\Delta t)^2\right] + O\left[(\Delta x)^2\right]$$

This equations means that the value of a electric or magnetic field at a given point in space and a given point in time depends only on previous time and space steps calculations, which are stored in memory. Hence by knowing the initial conditions of the modeled system, FDTD is an efficient and recursive way to compute electromagnetic fields.

3) The Yee Algorithm

From reference [3] it is observed that when considering three dimensional models, Kane Yee, the original pioneer of FDTD, came up with an elegant and robust solution: the Yee Algorithm. The main idea of the Yee algorithm is that it chooses a geometric relation for the sampling of electric and magnetic fields components that accurately represents Maxwell's equation both in differential and integral forms.

The basis of the FDTD numerical algorithm for three dimensional objects interactions is a system of six scalar equations derived from Maxwell's curl equations:

$$\frac{\partial H_x}{\partial t} = \frac{1}{\mu}\left[\frac{\partial E_y}{\partial z} - \frac{\partial E_z}{\partial y} - \left(M_{\text{source}_x} + \sigma^* H_x\right)\right]$$

$$\frac{\partial H_y}{\partial t} = \frac{1}{\mu}\left[\frac{\partial E_z}{\partial x} - \frac{\partial E_x}{\partial z} - \left(M_{\text{source}_y} + \sigma^* H_y\right)\right]$$

$$\frac{\partial H_z}{\partial t} = \frac{1}{\mu}\left[\frac{\partial E_x}{\partial y} - \frac{\partial E_y}{\partial x} - \left(M_{\text{source}_z} + \sigma^* H_z\right)\right]$$

$$\frac{\partial E_x}{\partial t} = \frac{1}{\varepsilon}\left[\frac{\partial H_z}{\partial y} - \frac{\partial H_y}{\partial z} - \left(J_{\text{source}_x} + \sigma E_x\right)\right]$$

$$\frac{\partial E_y}{\partial t} = \frac{1}{\varepsilon}\left[\frac{\partial H_x}{\partial z} - \frac{\partial H_z}{\partial x} - \left(J_{\text{source}_y} + \sigma E_y\right)\right]$$

$$\frac{\partial E_z}{\partial t} = \frac{1}{\varepsilon}\left[\frac{\partial H_y}{\partial x} - \frac{\partial H_x}{\partial y} - \left(J_{\text{source}_z} + \sigma E_z\right)\right]$$

Where ε represents the electric permittivity, σ the electric conductivity of the source J and σ^* represents the equivalent magnetic loss of the source M. Yee's algorithm considers lossless materials, i.e. $\sigma = \sigma^* = 0$ and possesses a robust basis with the following characteristics:

- The Yee Algorithm solves both the electric and magnetic fields using Maxwell's coupled equations rather than solving independently E or H using a wave equation. Using both the information of E and H makes the algorithm more robust.
- The Yee Algorithm centers its E and H components in 3D space so that each E component is surrounded by four circulating H components and vice versa as shown in Figure 23.
- The Yee Algorithm centers E and H field components in time (Figure 24) Once the calculations for E have been made and the result stored in memory, H is computed according to this result. This cycle then repeats for E and so on.

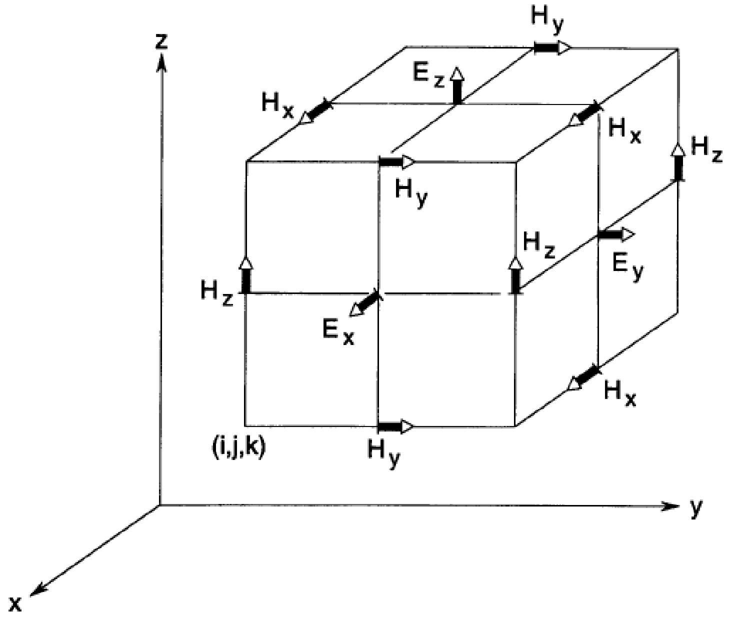

Figure 23 Position of the electric and magnetic field vector component about a cubic unit cell of the Yee space lattice [3]

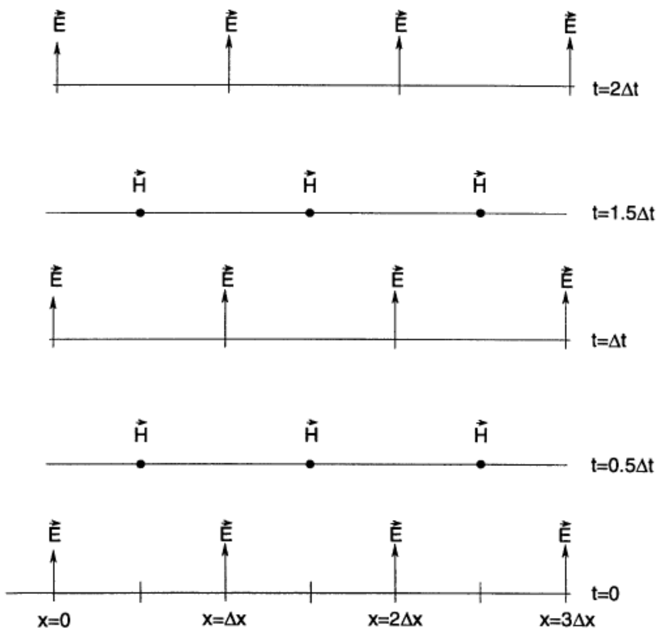

Figure 24 Space-time chart of the Yee algorithm for a one-dimensional wave propagation example showing the use of central differences for the space derivatives and leapfrog for the time derivatives. [3]

Much like seen in the one-dimensional case described above, Yee introduced a shorthand notation for three dimensional fields:

$$u(i\Delta x, j\Delta y, k\Delta z, n\Delta t) = u^n_{i,j,k}$$

Similarly to the one-dimensional case, Yee's algorithm uses the finite difference approximation (hence the name *FD*TD), only solving for the first order derivative instead of the second order:

$$\frac{du}{dx}(i\Delta x, j\Delta y, k\Delta z, n\Delta t) = \frac{u^n_{i+1/2,j,k} - u^n_{i-1/2,j,k}}{\Delta x} + O[(\Delta x)^2]$$

The use of half-space steps allows the algorithm to use stored values of fields surrounding the desired field. For example, computing a component of H separated of surrounding E field components by $\pm\Delta x/2$ can use those values, thanks to the finite difference approximation described above. By analogy, a similar approximation can be done for the time-step.

As shown in [3], via the finite differences described above and the semi-implicit approximation below:

$$u^n_{i,j,k} = \frac{u^{n+1/2}_{i,j,k} - u^{n-1/2}_{i,j,k}}{2}$$

It is possible to form an equation for each of the six scalar equation detailed above where the calculation of a field at time step $n + 1/2$ depends on E and H fields previously computed, at adjacent points. The equation below is an example of one of these equations:

$$H_z\Big|^{n+1}_{i,\,j+1,\,k+1/2} = \left(\frac{1 - \dfrac{\sigma^*{}_{i,\,j+1,\,k+1/2}\,\Delta t}{2\mu_{i,\,j+1,\,k+1/2}}}{1 + \dfrac{\sigma^*{}_{i,\,j+1,\,k+1/2}\,\Delta t}{2\mu_{i,\,j+1,\,k+1/2}}} \right) H_z\Big|^{n}_{i,\,j+1,\,k+1/2}$$

$$+ \left(\frac{\dfrac{\Delta t}{\mu_{i,\,j+1,\,k+1/2}}}{1 + \dfrac{\sigma^*{}_{i,\,j+1,\,k+1/2}\,\Delta t}{2\mu_{i,\,j+1,\,k+1/2}}} \right) \cdot \left(\begin{array}{l} \dfrac{E_x\Big|^{n+1/2}_{i,\,j+3/2,\,k+1/2} - E_x\Big|^{n+1/2}_{i,\,j+1/2,\,k+1/2}}{\Delta y} \\ - \dfrac{E_y\Big|^{n+1/2}_{i+1/2,\,j+1,\,k+1/2} - E_y\Big|^{n+1/2}_{i-1/2,\,j+1,\,k+1/2}}{\Delta x} \\ - M_{\text{source}_z}\Big|^{n+1/2}_{i,\,j+1,\,k+1/2} \end{array} \right)$$

4) Dispersion and stability

Dispersion can be viewed either as a variation of velocity *v* with regard of the frequency, or as a variation of wavelength λ according to frequency *f*. Dispersion can be represented as a variation of the wavenumber $k = 2\pi/\lambda$ with angular frequency $\omega = 2\pi f$.

In [3], it is shown that the numerical approximation $\tilde{k}$ of the volumetric components of the wave number *k* leads to dispersion. Ideal dispersion in three dimensional space is characterized by the following expression:

$$\left(\frac{w}{c}\right)^2 = {k_x}^2 + {k_y}^2 + {k_z}^2$$

This numerical dispersion can be diminished via two means:

- If the mesh (gridding) is sufficiently small, dispersion is greatly mitigated as the approximation of *k* approaches its real value.
- If a certain time step, called the Magic Time Step, is chosen. If we consider a cubic space lattice:

$$\tilde{k}_x = \tilde{k}_y = \tilde{k}_z = \tilde{k} / \sqrt{3}$$

[3] also shows that the time step must respect some criteria for the overall system to be stable. Outside this range, values grow exponentially and the system is deemed “unstable”:

$$\Delta t \leq \frac{1}{c\sqrt{\frac{1}{(\Delta x)^2} + \frac{1}{(\Delta y)^2} + \frac{1}{(\Delta z)^2}}}$$

III – Finding the appropriate brick

One of the most important aspects of this research and the first step of the simulation process was to define a reference brick that could be used by telecommunications engineers to simulate the impact of the human hand on the quality of their antenna design. In order to achieve this reference brick, a certain number of assertions had to be made:

- As the design was to be as simple as possible, the human hand was considered as a single layer object, so the bone, flesh or fat's particular impact on power dissipation was not considered. However, this was the topic of a side experiment described in the chapter above.
- An AAU3-compatible design (Figure 25) for the human hand was taken from the PhD of Mauro Pelosi, our supervisor [1]. This design however was not simple enough for the study intended.

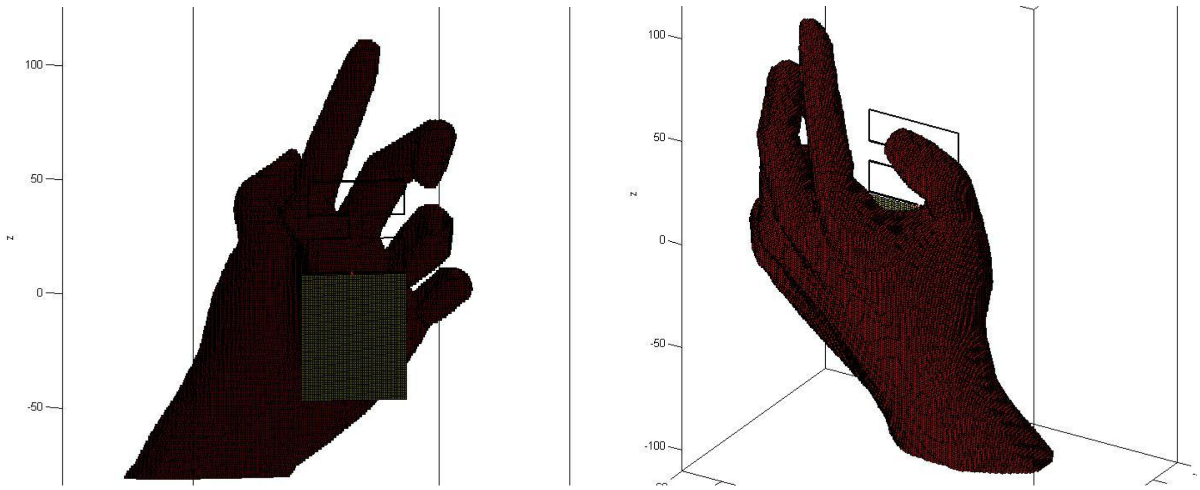

Figure 25 An AAU3 human hand design

The key factor for the acceptation of the reference brick that would become our human hand proxy was that the total power dissipated was identical between the brick and the hand. This simplification has limits, of course, as the power dissipated calculated along the axes is of course a very rough estimation.

The hand being rather thin (from 1 to 3 centimeters at maximum), the brick should also not be cubic but rather thin.

To find the appropriate brick, we started to do the simulation with a brick which has globally the same height, width and length as the hand. After, we decreased each parameters, methodically, to obtain the closest value as possible of power dissipated compared to the value simulated with the hand.

The results of these tests are on the next table:

Brick	Input power	Radiated power	Dissipated power	Error with the ref. dissipated power
1	2,33E-09	8,78E-10	1,45E-09	1,01E-10
2	2,49E-09	4,06E-10	2,08E-09	7,27E-10
3	2,24E-09	2,03E-10	2,03E-09	6,79E-10
4	2,49E-09	4,07E-10	2,09E-09	7,32E-10
5	2,41E-09	3,89E-10	2,02E-09	6,70E-10
6	2,80E-09	3,65E-10	2,44E-09	1,08E-09
7	1,38E-09	4,91E-10	8,85E-10	-4,68E-10
8	2,20E-09	3,90E-10	1,81E-09	4,57E-10
9	2,30E-09	3,96E-10	1,90E-09	5,48E-10
10	2,36E-09	3,79E-10	1,98E-09	6,24E-10
11	1,37E-09	4,15E-10	9,53E-10	-4,00E-10
12	1,44E-09	3,77E-10	1,07E-09	-2,87E-10
13	1,62E-09	3,69E-10	1,25E-09	-9,83E-11
14	1,88E-09	3,79E-10	1,50E-09	1,50E-10
15	1,53E-09	3,70E-10	1,16E-09	-1,97E-10
16	1,74E-09	3,73E-10	1,37E-09	1,62E-11

Table 6 Results of the simulations of different test bricks

In the end, a brick corresponding to the different criterions with dimensions of 22mm x 52mm x 106mm, was chosen. The following figure is showing the design of this hand.

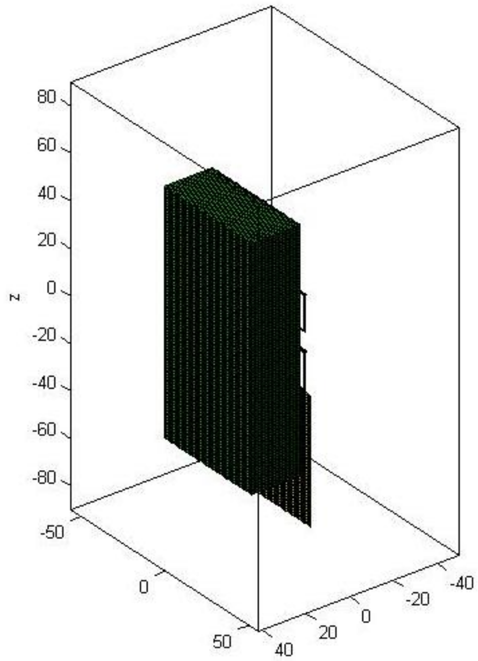

Figure 26 The simplified human hand model

IV – Difference in power calculation

As described in chapter two, there are two methods of calculation for the total power dissipated. One approach, used by the AAU3 software, is via the computation of the pointing vector. The other is a more down-to-earth method and specific to FDTD, by doing the summation of the power dissipation of each cell.

While using both techniques in simulations, results differed according to the method used, which led to some questioning about whether one or the other technique was not correctly implemented. However, it turned out that both were correct, therefore some research has been done with the aim of predicting the difference between the two methods. Using the same simulation as the "Conductivity, permittivity and permeability variations" side experiment, we obtained the results in Table 7 below.

Sigma	Mu	Epsilon	Pdis C by C	Pdis AAU3	%Err
0,85	1	42,5	8,34E-10	8,53E-10	2,24
1	1	42,5	8,52E-10	8,71E-10	2,22
2	1	42,5	8,05E-10	8,27E-10	2,65
3	1	42,5	7,11E-10	7,36E-10	3,33
4	1	42,5	6,34E-10	6,59E-10	3,82
1	1	1	1,04E-09	1,07E-09	2,74
1	1	1,5	1,05E-09	1,08E-09	2,72
1	1	2	1,06E-09	1,09E-09	2,69
1	1	10	1,11E-09	1,14E-09	2,44
1	1	20	1,05E-09	1,07E-09	2,18
1	1	30	9,04E-10	9,24E-10	2,21
1	2	42,5	1,10E-09	1,12E-09	2,26
1	4	42,5	1,48E-09	1,52E-09	2,68

Table 7 Error calculation between computation techniques

While the error is always small, it seems as though the smaller the total power dissipation is, the higher the error is. The conclusion is that there might be a "static" error diminishing with large numbers. However, we could not prove this hypothesis.

CHAPTER FOUR: COMPARISON OF REFERENCE ANTENNAS

I – Introduction

This chapter will present the simulation results and an interpretation on each of these results.

During the simulation process, we have proceeded in the following manner for every antenna: firstly we have designed the antenna in free space, then we have run another simulation with a brick and finally we have made a comparison of the different results.

Also, in order to obtain the most relevant results, we have applied the following rules to every simulation we launched:

- The domain of the simulation has a fixed size of 92 x 112 x 180mm
- The antenna is designed to be resonant at a frequency of 1GHz
- We used the brick defined in the previous chapter
- The antenna is located at 10mm from the brick on the x-axis
- The position of the antenna on the y and z axis is determined in such way that the antenna is centered in comparison with the brick

For each type of antenna, the following parameters are going to be presented and analyzed in the next parts:

- A comparison graph of the S11 curves (without and with the brick)
- The 3D correlation coefficient between the 2 simulations
- The Power dissipated along the x-axis
- The percentage of power dissipated in the brick regarding to the input power
- The efficiency parameter

II – Antennas

1) Antenna definition [14]

An antenna is the basic communication device in a wireless system, acting as a transceiver or a receiver. Ideally, thanks to the reciprocity theorem, the behavior of the antenna in these two modes is identical (However it might not be the case if the antenna is in a non linear/isotropic/non-dispersive medium). An antenna's aim is to convert an induced current into a radio frequency and vice versa.

2) Antenna parameters

An antenna has several defining characteristics, which are developed below:

- The radiation pattern

From Antenna Theory [14], the radiation pattern can be defined as "*a mathematical or graphical representation of the radiation properties of the antenna as a function of space coordinates.*"

The radiation pattern is a tool used to visualize the power transmitted of received by an antenna as a function of the angle and the distance at which the receiver or transceiver is located. Usually, the radiation pattern of antennas is divided in lobes (main, side, back), which are regions of certain radiation intensity. Side lobes are usually minimized to optimize the directivity of the antenna.

- Field regions

The area around an antenna is divided in three regions. The reactive near-field is defined when the radial distance is $R < 0.62\sqrt{\frac{D^3}{\lambda}}$, where D is the antennas largest dimension. In this region, the waves are highly unstable and it is where most power is stored before being sent. The radiating near-field (Fresnel) region is defined when the radial distance is $0.62\sqrt{\frac{D^3}{\lambda}} < R < \frac{2D^2}{\lambda}$. Finally, the far field (Fraunhofer) region is defined where $R > \frac{2D^2}{\lambda}$. In this last region, wave fronts are considered as spherical.

- Directivity

From Antenna Theory [14], directivity is defined as "*the ratio of the radiation intensity in a given direction from the antenna to the radiation intensity averaged over all directions, where the average radiation intensity is the total power radiated from the antenna divided by 4π*".

$$D = \frac{U}{U_0} = \frac{4\pi U}{P_{rad}}$$

When considering no particular direction, U is considered as its maximum value.

- Antenna efficiency

Antenna efficiency is the ratio of the power radiated by the antenna over the input power it is given. The total efficiency depends on the reflection efficiency (mismatch between the antenna and the transmission line), the conduction efficiency and the dielectric efficiency.

$$e_0 = e_r e_c e_d$$

- Gain

From Antenna Theory [14], gain is defined as "*the ratio of the intensity in a given direction to the radiation intensity that would be obtained if the power accepted by the antenna were radiated isotropically".* Gain relates the efficiency and the directivity of the antenna.

$$G = 4\pi \frac{U(\theta,\varphi)}{P_0}$$

- Bandwidth

From Antenna Theory [14], bandwidth is defined as "*the range of frequencies within which the performance of the antenna with respect to some characteristic conforms to a specified standard"*. Bandwidth can have several definitions, like Half Power Bandwidth, or Peak to Null Bandwidth.

III – Dipole

1) Presentation

The first antenna to be simulated was a half-wavelength dipole antenna. A dipole antenna consists of 2 aligned wires separated by a central feeding element.

The "half-wavelength" term means that the dipole is composed of two quarter wavelength conductors and thus the total length of this antenna is equal to a half-wavelength at the simulated frequency. This type of dipole is commonly used due to the fact that the matching is simplified because of a radiation resistance of 73 ohms.

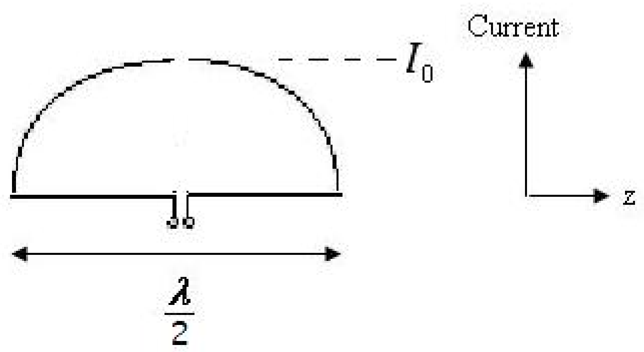

Figure 27 Electric current on a half wavelength dipole [17]

During the simulation process, at the operational frequency of 1GHz, the total length of the antenna was equal to 150mm.

The designs of the simulated environments are presented on the following schemes:

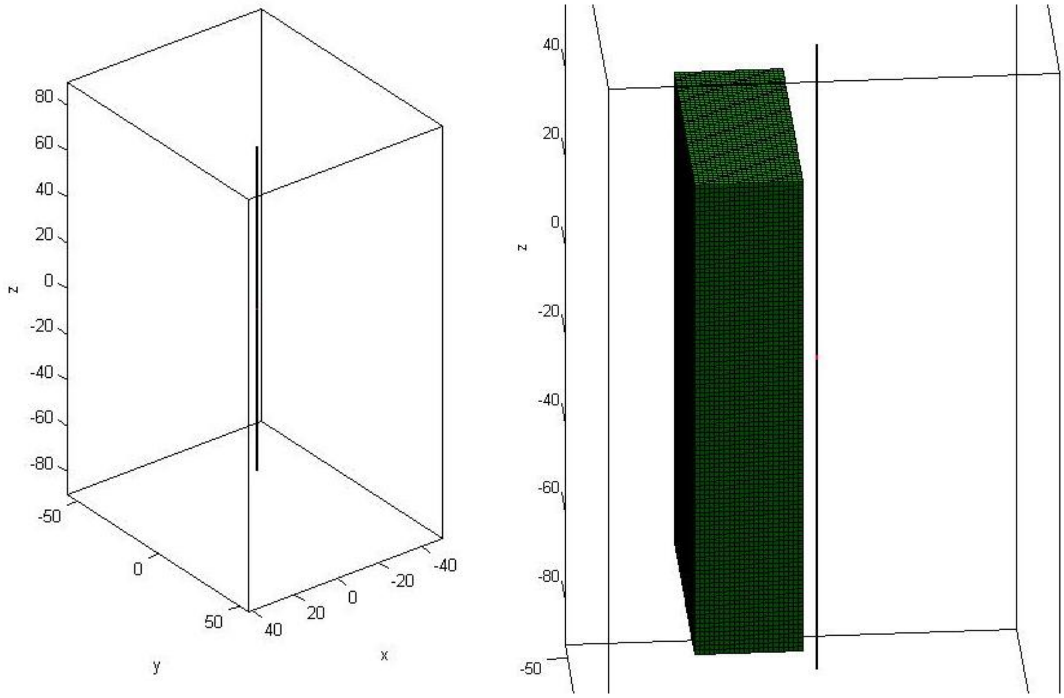

Figure 28 Design of a dipole antenna in free space (left) and facing a human-hand-like dissipative brick (right)

2) Results of the robustness experiment

The following graph is presenting the evolution of the s11 parameter in function of the frequency for both cases, in free space and with the brick.

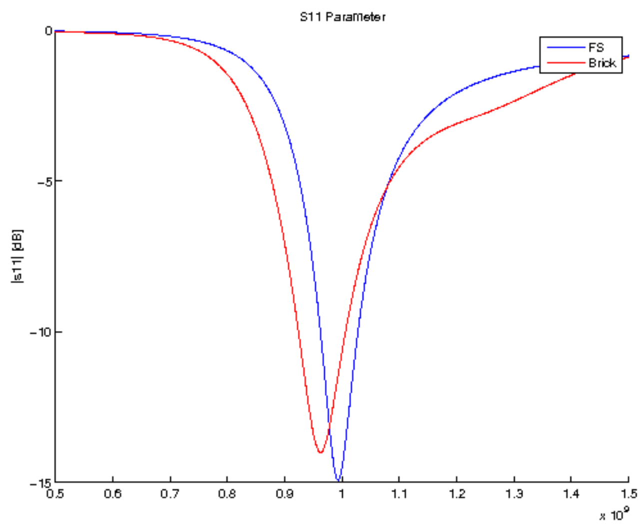

Figure 29 Impact of the human-hand-like brick on the S11 parameter of the dipole antenna

The brick has a very limited influence on the amplitude of the reflection coefficient (-14dB with the brick, -15dB without) and the shift of the resonant frequency (963MHz vs 994MHz) is one of the smallest in this study, as it is only 31MHz. However, after the insertion of the brick, the bandwidth has been significantly increased by 50% (146MHz in free space and 216MHz with the brick).

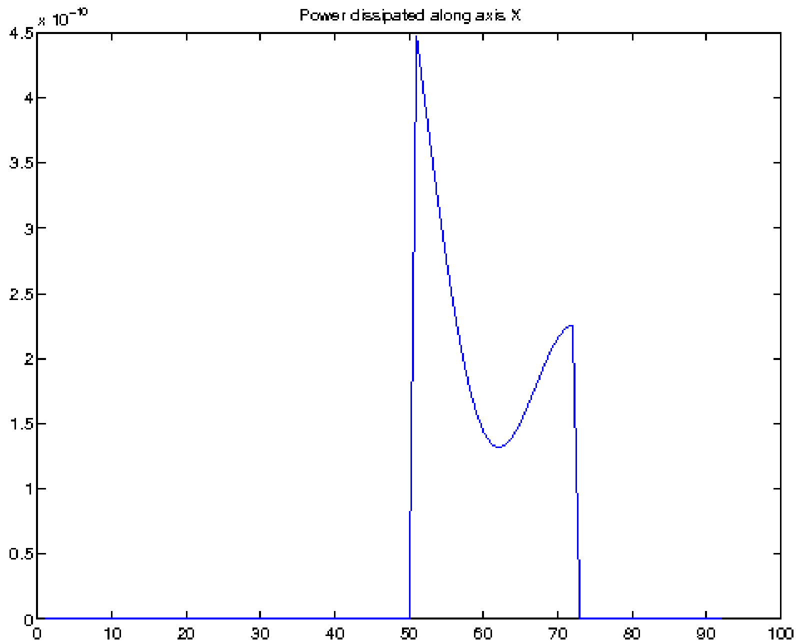

Figure 30 Dissipation along the radial axis of a dipole antenna facing a 22mm-wide human-hand-like brick

This graph shows that the highest dissipation ($4.5*10^{-10}$ W) occurs at the contact of the fields with the brick, then decreases until the center of the brick is reached to a minimum value of $1.3*10^{-10}$ W and finally increases again to attain a value of $2.3*10^{-10}$ W. The dipole antenna dissipates most of its input power at the beginning of the brick, unlike other antennas which spread an important part of the power dissipation at the rear of the brick (62% of the total power dissipated is dissipated in the first half of the brick). The total power dissipated is equal to $4.83*10^{-9}$ W, representing 67% of the input power.

The 3D correlation coefficient is at 0.94, one of the highest, which means that the fields of the dipole when considering the human hand are highly predictable.

3) Conclusion

While the reflection coefficient of the dipole is fairly robust to the impact of the human hand and while its high correlation coefficient makes it a predictable antenna, the half-wavelength dipole antenna dissipates one of the highest amounts of power in the hand, making it lossy. Another difficulty facing the monopole antenna is the size requirements to implement it on an actual mobile phone.

III – Monopole

1) Presentation

The monopole antenna can be described as a half of a dipole antenna mounted above a ground plane. The reflection theorem makes it the pendant of a half-wavelength dipole.

As a consequence, the impedance of the monopole antenna corresponds to one half of the impedance of the dipole antenna. In our case, the impedance of our quarter wavelength monopole equals to half of the impedance of the previously described half-wavelength antenna.

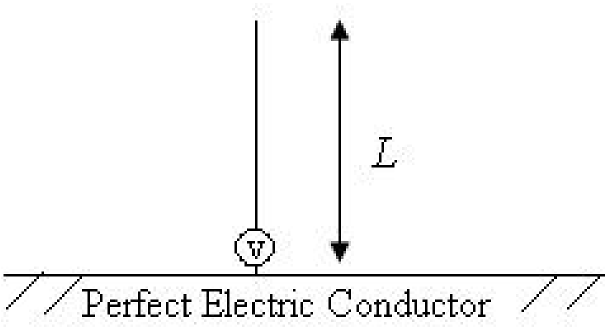

Figure 31 Monopole antenna of length L mounted above an infinite ground plane [18]

During our simulation, and at an operational frequency of 1GHz, we have designed a monopole antenna with the following characteristics:

- A length of 75mm
- A ground plane of dimensions 40mm*100mm

The designs of the simulated environments are presented on the following diagrams:

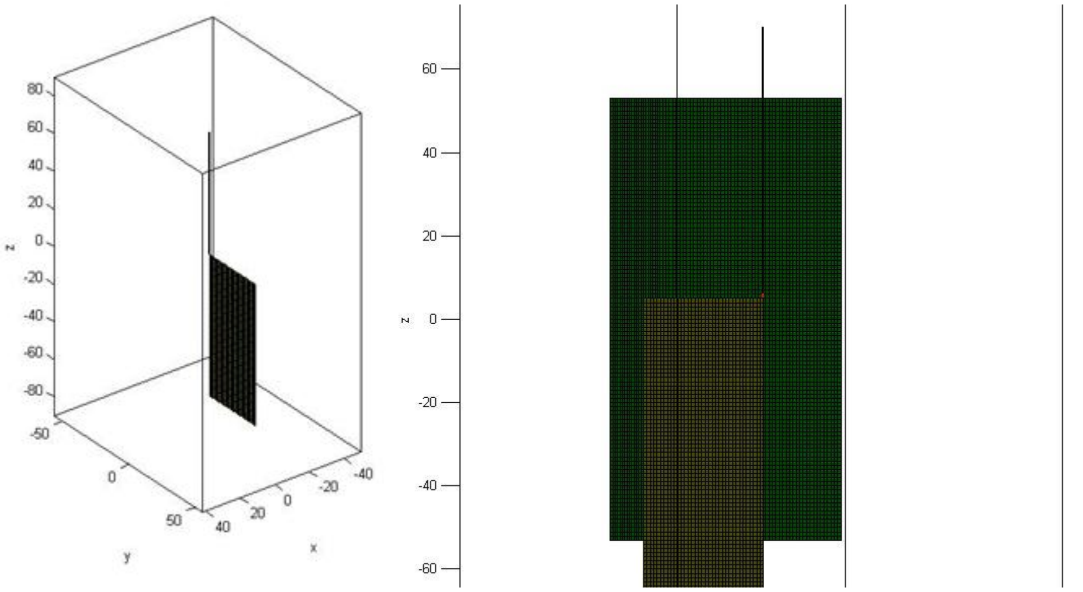

Figure 32 Design of a monopole antenna in free space (left) and facing a human-hand-like dissipative brick (right)

2) Results of the robustness experiment

The following graph is presenting the evolution of the s11 parameter in function of the frequency for both cases, in free space and with the brick.

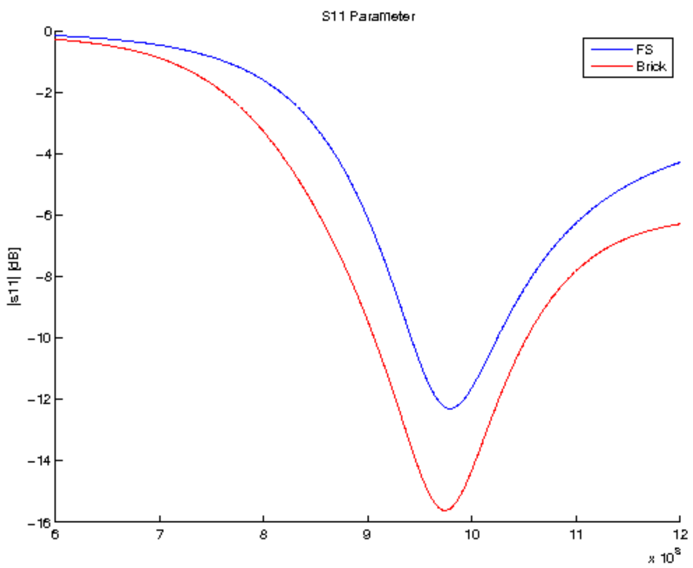

Figure 33 Impact of the human-hand-like brick on the S11 parameter of the monopole antenna

The resonant frequency of the monopole is not affected by the brick, but the S11 parameter at this frequency has been improved, evolving from -12dB to -15B. There is also a growth of the bandwidth after the insertion of the brick (291MHz without the brick and 339MHz with it). Overall, the monopole seems to benefit from the impact of the brick. Its bandwidth is increased, its resonant frequency is left untouched and its reflection coefficient decreases, making it more robust.

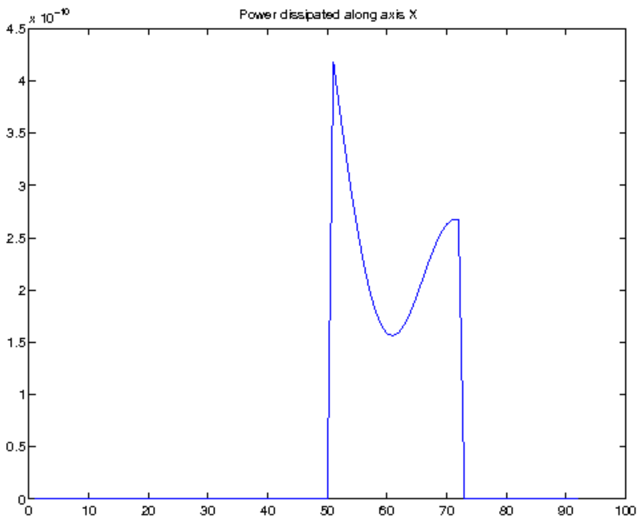

Figure 34 Dissipation (in W) along the radial axis of a monopole antenna facing a 22mm-wide human-hand-like brick

The behavior of the monopole antenna is similar to the one of the dipole antenna. In other terms, most of the dissipation ($4.3*10^{-10}$ W) occurs at the contact of the fields with brick, then decreases until the center of the brick is reached ($1.7*10^{-10}$ W) and finally increases again to attain $2.8*10^{-10}$ W. However there is a difference in that the ratio of front-to-rear power dissipated is lower in the case of the monopole. The total power dissipated is $5.21*10^{-9}$ W, representing 69% of the input power. With a dissipated power in the first half of the brick of $2.93*10^{-9}$ W (57% of the total dissipated power), there is almost an equal repartition of the dissipation.

The correlation coefficient between these 2 simulations is 89%, meaning that the monopole antenna is slightly less predictable than the dipole antenna when considering the brick.

3) Conclusion

The monopole antenna has some pros to it, when placed near the human-hand-like brick, its resonant frequency does not vary, its bandwidth increases and its reflection coefficient lowers. However, the percentage of input power dissipated is one of the highest in this study, making it a lossy antenna.

IV – PIFA

1) Presentation

The Planar Inverted F Antenna (PIFA) is a micro strip antenna commonly used in mobile phone. It is composed of a top patch, a ground plane, a feeding pin and a shorting pin, as shown on the next scheme:

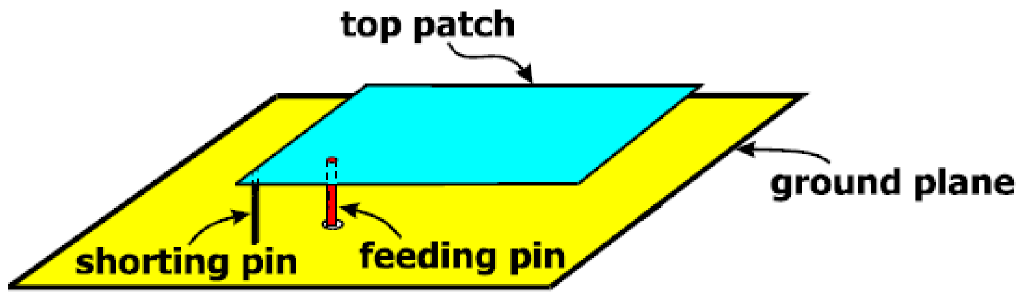

Figure 35 General design of a PIFA [21]

The top patch can be printed on a substrate and can also be folded. These two cases will be explored in the next paragraph.

The PIFA is resonant at a frequency of a quarter wavelength, which means that the sum of the length and the width of top patch of the antenna is $\lambda/4$ (because in the case developed in this report, the short pin is only a wire).

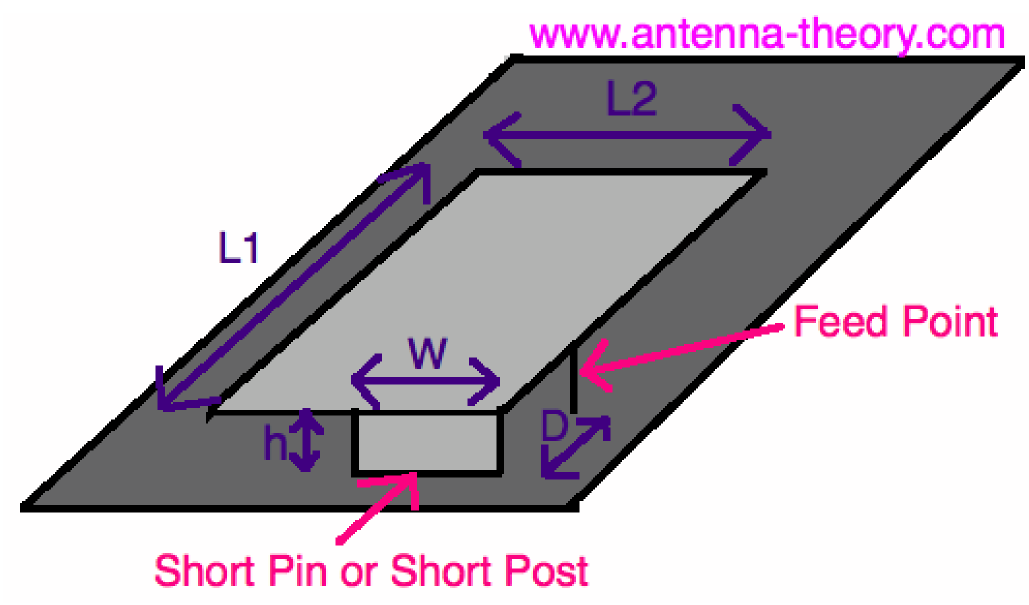

Figure 36 Dimensions of a PIFA [22]

The size of the PIFA can be defined based on the notations of the previous scheme:

$$L1+L2-W=\lambda/4$$

The distance between the feeding point and the short pin and the distance between the ground plane and the superior part are important for the bandwidth and the impedance. When the distance between the feeding pin and the shorting pin decrease, the impedance decrease, and inversely, when the distance increase, the impedance increase too.

This antenna is common in mobile phone because of its low profile and its omnidirectional pattern.

The designs of the simulated environments are presented on the following diagrams:

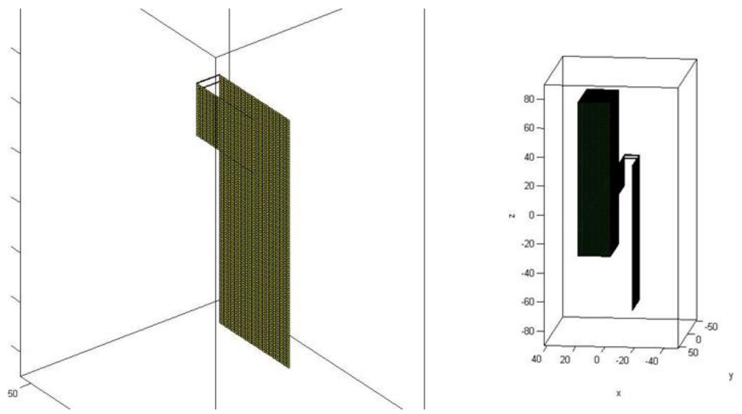

Figure 37 Design of a PIFA antenna in free space (left) and facing a human-hand-like dissipative brick (right)

2) Results of the robustness experiment

The following graph is presenting the evolution of the s11 parameter in function of the frequency for both cases, in free space and with the brick.

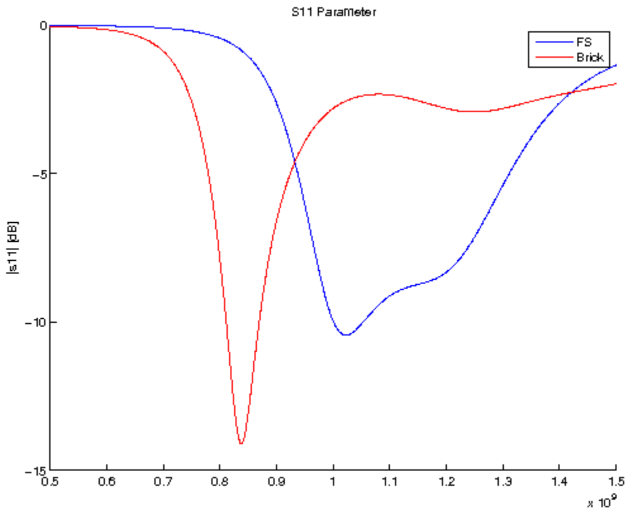

Figure 38 Impact of the human-hand-like brick on the S11 parameter of the PIFA

When considering the reflection coefficient of the PIFA, the influence of the human hand can be characterized as such:

- The overall value of the reflection coefficient at the resonant frequency varies from -10.45dB in free space to -14.11dB with the presence of the brick. At the desired frequency of 1GHz, the reflection coefficient of the PIFA with the brick rises to -2.5dB, making it very vulnerable to interference and thus a poor choice for an antenna.
- The resonant frequency sets to 838MHz instead of the designed 1.02GHz (185MHz variation).
- The bandwidth of the PIFA in free space is 10 944MHz, and 708MHz with the brick. This represents an important variation of 93.53%.

Power dissipation along x:

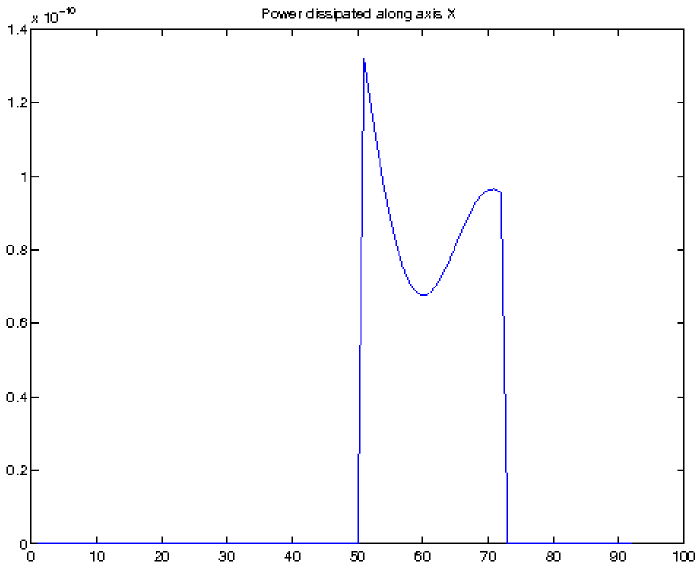

Figure 39 Dissipation (in W) along the radial axis of a PIFA antenna facing a 22mm-wide human-hand-like brick

This graph shows that most of the dissipation occurs at the contact of the brick, and then decreases from $1.3*10^{-10}$ W to $0.7*10^{-10}$ W until the center of the brick is reached and finally increases to attain the value of $0.98*10^{-10}$ W. The total power dissipated is $1.93*10^{-9}$ W, representing 51.63% of the input power. With a dissipated power in the first half of the brick of $1.05*10^{-9}$ W (54% of the total dissipated power), there is almost an equal repartition of the dissipation.

3) Conclusion

While the PIFA antenna in free space obviously suffers from a flaw in design, the presence brick manages to correct it. With relatively low input power dissipation (51%) and a good reflection coefficient value, the PIFA antenna appears as one of the most robust antennas of this study.

V – Slotted PIFA

1) Presentation

As said previously, the top patch of the PIFA can be slotted. This technique is used to reduce the size of the top patch. In this case, the important parameter is not the area of the patch, but its perimeter.

The designs of the simulated environments are presented on the following diagrams:

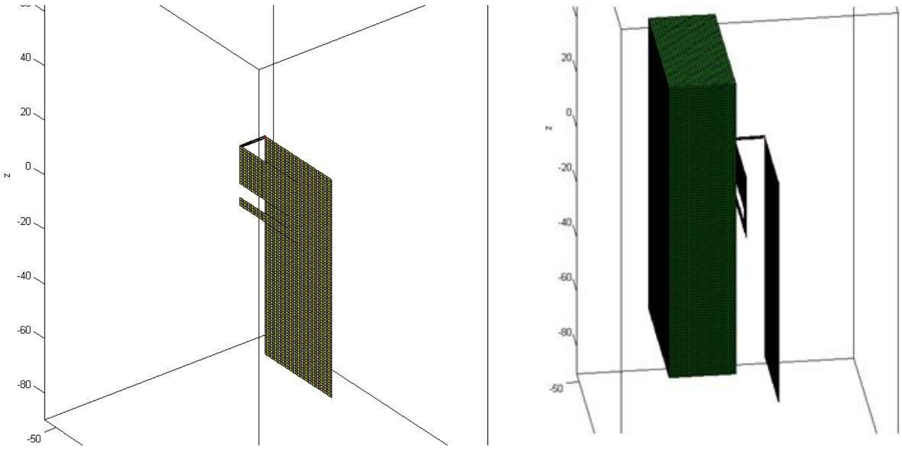

Figure 40 Design of a slotted PIFA antenna in free space (left) and facing a human-hand-like dissipative brick (right)

2) Result of the robustness experiment

The following graph is presenting the evolution of the s11 parameter in function of the frequency for both cases, in free space and with the brick.

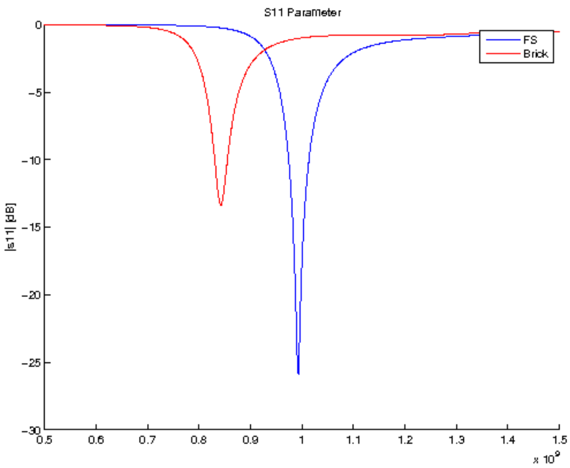

Figure 41 Impact of the human-hand-like brick on the S11 parameter of the slotted PIFA

When considering the reflection coefficient of the slotted PIFA, the influence of the human hand can be characterized as such:

- The overall value of the reflection coefficient at the resonant frequency varies from -25.88dB in free space to -14.11dB with the presence of the brick. At the desired frequency of 1GHz, the reflection coefficient of the slotted PIFA with the brick rises to -1dB, making it totally vulnerable to interference and thus a poor choice for an antenna.
- The resonant frequency sets to 842MHz instead of the designed 993GHz (151MHz variation).
- The bandwidth of the slotted PIFA in free space is 332MHz, and 83MHz with the brick. This represents an important variation of 75.07%.

Power dissipation along x:

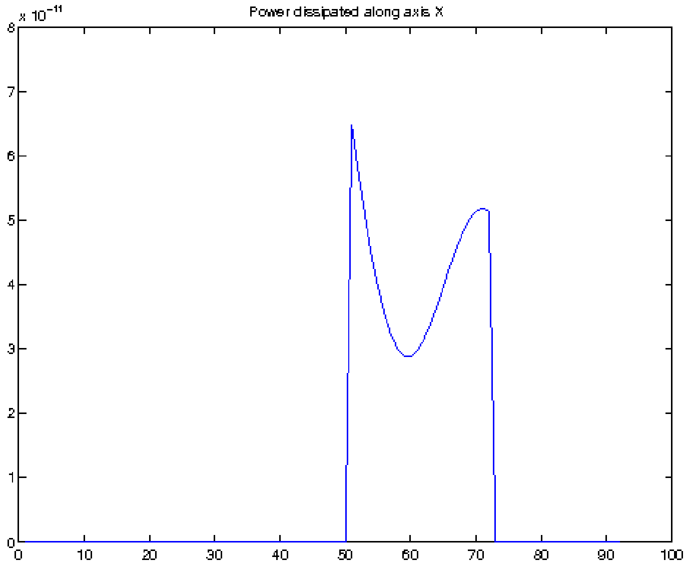

Figure 42 Dissipation (in W) along the radial axis of a slotted PIFA facing a 22mm-wide human-hand-like brick

This graph shows that most of the dissipation occurs at the contact of the brick, then decreases from $6.8*10^{-11}$ W to $3*10^{-11}$ W until the center of the brick is reached and finally increases again until $5.2*10^{-11}$W. The front-to-rear ratio of power dissipation is one of the lowest in this study. The total power dissipated is 9.25e-10 W, representing 58.80% of the input power. With a dissipated power in the first half of the brick of 4.74e-10 W (51%

of the total dissipated power), there is almost an equal repartition of the dissipation.

3) Conclusion

The slotted PIFA antenna is much impacted from the presence of the human hand in its vicinity. Its resonant frequency is shifted by 200MHz, its reflection coefficient increases by 12dB.

VI – Narrowband PIFA

1) Presentation

In order to decrease the S11 and the bandwidth, the distance between the top patch and the ground plane can be reduced, resulting in a narrowband PIFA.

The designs of the simulated environments are presented on the following diagrams:

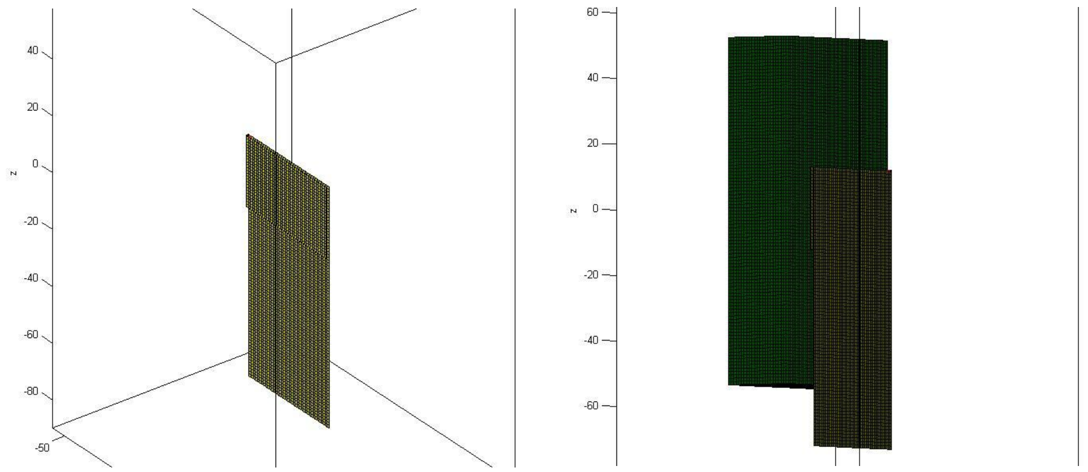

Figure 43 Design of a narrowband PIFA antenna in free space (left) and facing a human-hand-like dissipative brick (right)

2) Results of the robustness experiment

The following graph is presenting the evolution of the s11 parameter in function of the frequency for both cases, in free space and with the brick.

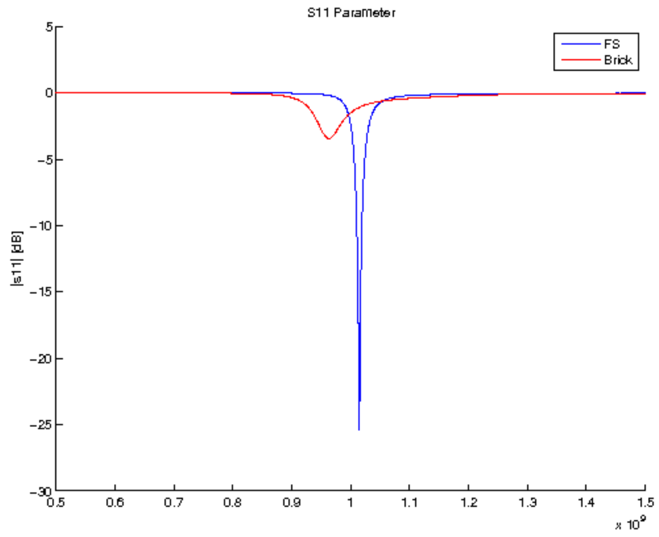

Figure 44 Impact of the human-hand-like brick on the S11 parameter of the narrowband PIFA

When considering the reflection coefficient of the narrowband PIFA, the influence of the human hand can be characterized as such:

- The overall value of the reflection coefficient at the resonant frequency varies from -25.37dB in free space to -3.44dB with the presence of the brick. At the desired frequency of 1GHz, the reflection coefficient of the narrowband PIFA with the brick rises to -1.5dB, making it totally vulnerable to interference and thus a poor choice for an antenna.

- The resonant frequency sets to 963MHz instead of the designed 1.02GHz (52MHz variation).

- The bandwidth of the PIFA in free space is 15MHz, and 260MHz with the brick. This represents a 1657.47% variation, which is an outlier.

Power dissipation along x:

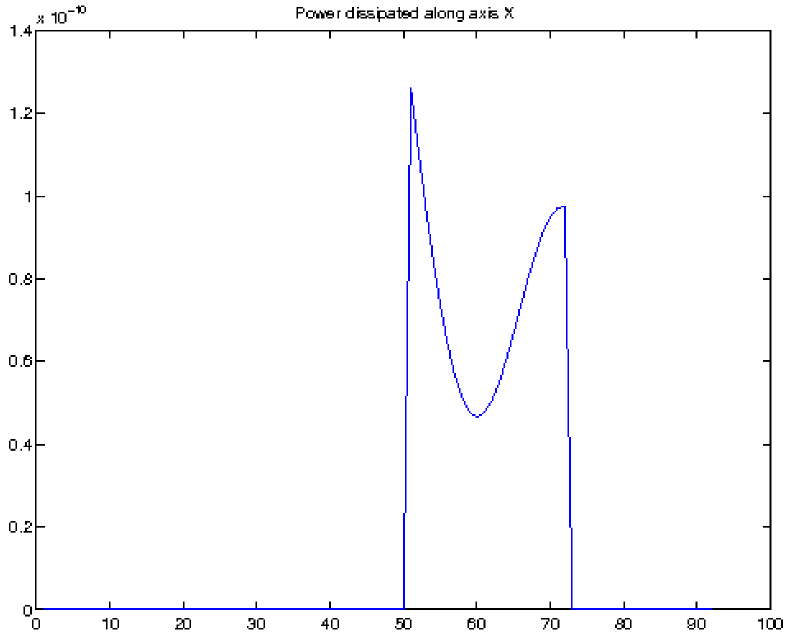

Figure 45 Dissipation along the radial axis of a narrowband PIFA facing a 22mm-wide human-hand-like brick

This graph shows that most of the dissipation occurs at the contact of the brick, and then decreases from $1.3*10^{-10}$ W to $0.48*10^{-10}$ W until the center of the brick is reached and finally increases again until $1*10^{-10}$ W. The spread between the front and rear of the brick is small. With a dissipated power in the first half of the brick of 8.59e-10 W (52% of the total dissipated power); there is almost an equal repartition of the dissipation. The total power dissipated is 1.66e-09 W, representing 72.51% of the input power.

The correlation coefficient between these 2 simulations is 93%, meaning that the impact of the human hand still makes the fields of the narrowband PIFA predictable.

3) Conclusion

Much like the slotted PIFA, the narrowband PIFA is greatly affected by the presence of the human hand. Its reflection coefficient greatly increases, to the point where the antenna is made very sensitive to transmission interference. Also, its resonant frequency is shifted by almost 100MHz.

VII – PIFA with substrate

1) Presentation

Substrates with high dielectric constant (Er) store energy and the PIFA with substrate is like a lossy capacitor with high Er and high quality factor, which reduce the bandwidth. Inversely, when the thickness of substrate increases, the capacitance decrease the energy stored and the quality factor. So the substrate is used to increase the bandwidth.

The designs of the simulated environments are presented on the following diagrams:

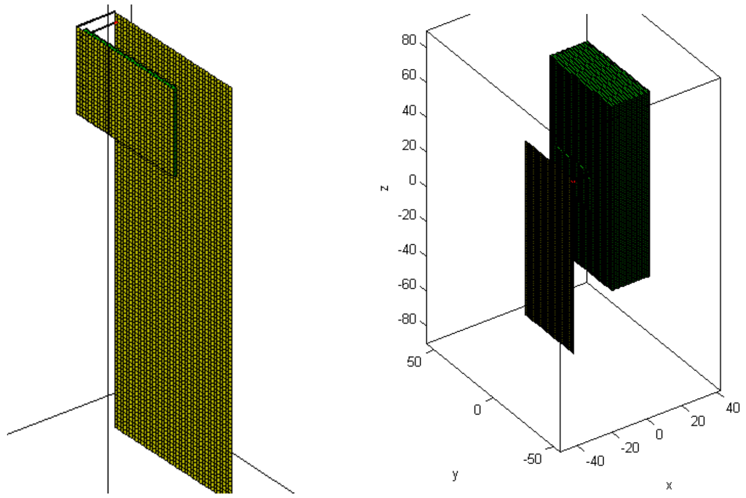

Figure 46 Design of a substrate PIFA antenna in free space (left) and facing a human-hand-like dissipative brick (right)

2) Results of the robustness experiment

The following graph is presenting the evolution of the s11 parameter in function of the frequency for both cases, in free space and with the brick.

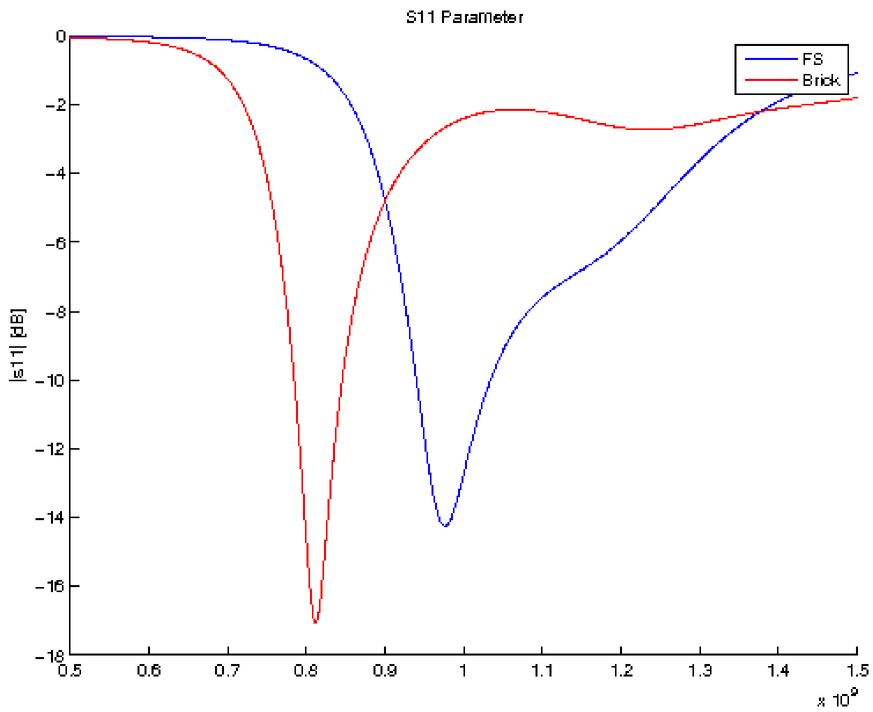

Figure 47 Impact of the human-hand-like brick on the S11 parameter of the PIFA with substrate

When considering the reflection coefficient of the PIFA with substrate, the influence of the human hand can be characterized as such:

- The overall value of the reflection coefficient at the resonant frequency varies from -13.97dB in free space to -17.07dB with the presence of the brick. At the desired frequency of 1GHz, the reflection coefficient of the PIFA with the brick rises to -2.4dB, making it very vulnerable to interference and thus a poor choice for an antenna.
- The resonant frequency sets to 812MHz instead of the designed 985GHz (173MHz variation).
- The bandwidth of the PIFA in free space is 914MHz and 1155MHz with the brick. This represents a 26.36% variation.

Power dissipation along x:

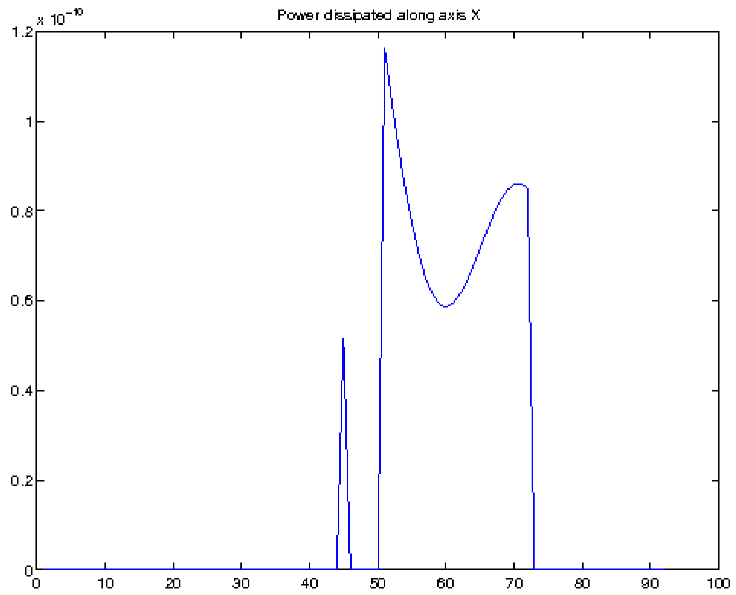

Figure 48 Dissipation (in W) along the radial axis of a PIFA with substrate facing a 22mm-wide human-hand-like brick

This graph shows that most of the dissipation occurs at the contact of the brick, and then decreases from $1.98*10^{-10}$ W to $0.59*10^{-10}$ W until the center of the brick is reached and finally increases again until $0.89*10^{-10}$W. There is also a peak of dissipation of $0.54*10^{-10}$ W before the brick, which is due to the layer of substrate. With a dissipated power in the first half of the brick of $9.14*10^{-10}$ W (52% of the total dissipated power), there is almost an equal repartition of the dissipation. The total power dissipated is $1.66*10^{-9}$ W, representing 72.51% of the input power.

3) Conclusion

While the presence of the human hand improves the reflection coefficient of the PIFA with substrate, its resonant frequency is shifted by 200MHz, which is a high amount. The PIFA with substrate also dissipates 72% of its input power in the hand, making it one of the most dissipative antennas in this survey.

VIII – IFA

1) Presentation

The inverted-F antenna is often described as a 2D PIFA antenna.

The following diagram is describing the geometry of this antenna [20] :

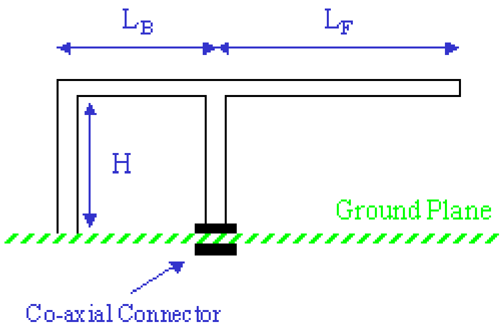

Figure 49 Dimensions of an IFA antenna

- H is the height of the horizontal element above the ground plane
- LF is the horizontal length from the feed point to the open end of the antenna
- LB is the horizontal length from the feed point to the closed end of the antenna

During our simulation, and at an operational frequency of 1GHz, we have designed an IFA antenna with the following characteristics:

- A total length (LB + LF) of 43mm
- A distance of 5mm from the feed point to the closed end of the antenna (LB)
- A height of 18mm for the horizontal element (H)
- A ground plane of dimensions 44*60mm

The designs of the simulated environments are presented on the following diagrams:

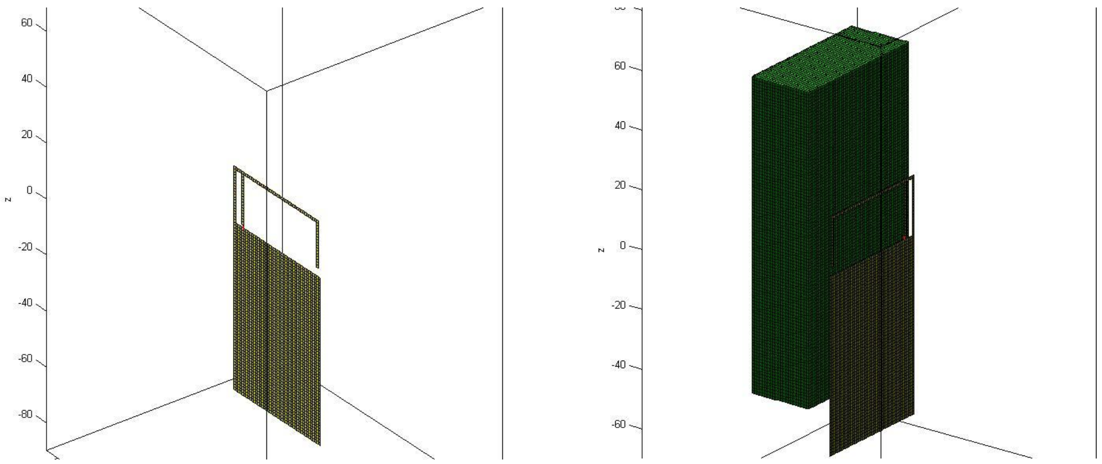

Figure 50 Design of an IFA antenna in free space (left) and facing a human-hand-like dissipative brick (right)

2) Results of the robustness experiment

The following graph is presenting the evolution of the s11 parameter in function of the frequency for both cases, in free space and with the brick.

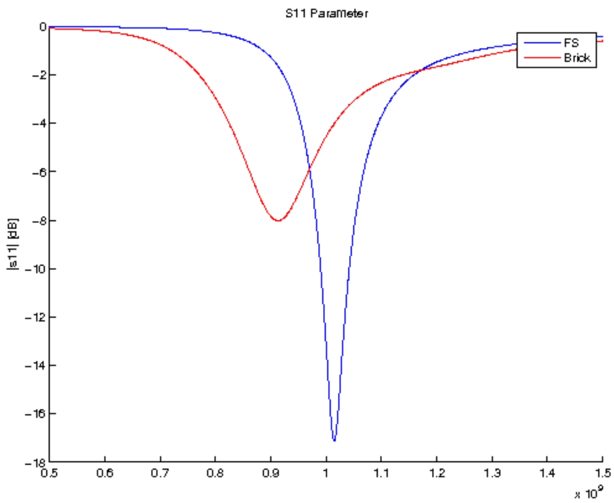

Figure 51 Impact of the human-hand-like brick on the S11 parameter of the IFA antenna

This graph is clearly showing that the brick has a serious impact on the S11 parameter. The resonant frequency has been moved from 1GHz (in free space) to 900MHz (brick scenario) and the reflection coefficient parameter has evolved respectively from -17dB to -8dB.

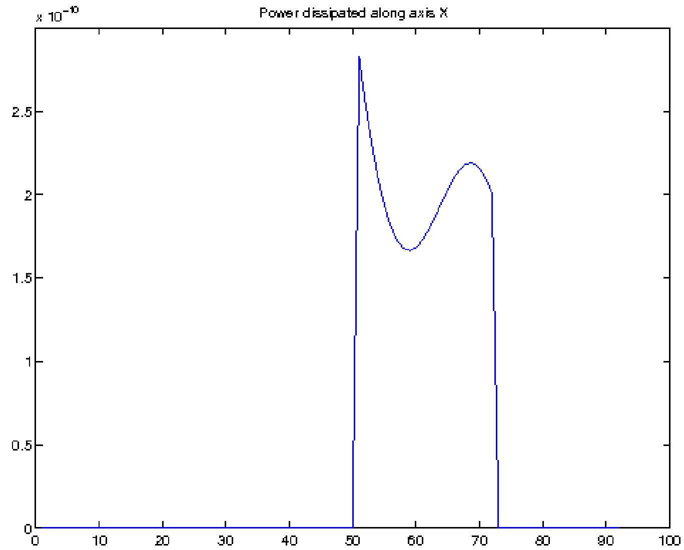

Figure 52 Dissipation along the radial axis of an IFA antenna facing a 22mm-wide human-hand-like brick

This graph shows that the highest dissipation occurs at the contact of the fields with the brick ($2.8*10^{-10}$ W), then decreases until the center of the brick is reached and finally increases again to attain a value of $2.3*10^{-10}$ W. The power dissipated in the first 1.1 centimeters being $2.38*10^{-9}$ W (53% of the total power dissipated), there is almost an equal repartition of the dissipation. The total dissipated power is $4.45*10^{-9}$ W, representing 88% of the input power.

3) Conclusion

The impact of the human hand on the performance of an inverted F antenna is considerable. Its resonant frequency is shifted by 100MHz, its reflection coefficient increases by a factor of 10 and the antenna dissipates 88% of its input power inside the human hand. The IFA is one of the less robust antennas in this survey.

IX – Loop

1) Presentation

The loop antenna is both simple in design, and simple in analysis, making it one of the most investigated antennas. The loop antenna can take a wide variety of geometries: circular, rectangular, triangular, elliptic, and in general sense polygonal. Figure 53 below shows a typical circular loop antenna.

Figure 53 A real-life implementation of a loop antenna [19]

Loop antennas are classified into two categories:

Electrically small loop antennas have an overall circumference (or length) of less than one-tenth of the sought wavelength ($C < \lambda/10$). These antennas can be shown to behave like an infinitesimal dipole and are poor radiators and are mostly used in receiving mode [4]. Because of this reason, this experiment does not consider the electrically small loop antenna.

Electrically large loop antennas have a circumference close to a wavelength ($C \sim \lambda$) and are typically used for frequency bands above 3MHz. In this study, an electrically large loop antenna is considered for the sake of being one of the most spread antennas on the market. This loop resonates at 1GHz.

The AAU3 software allows only cubic, planar or wire modeling of three-dimensional shapes. Hence the circular loop was deemed unfit for this tool, and a rectangular loop was designed as shown in Figure 54 below.

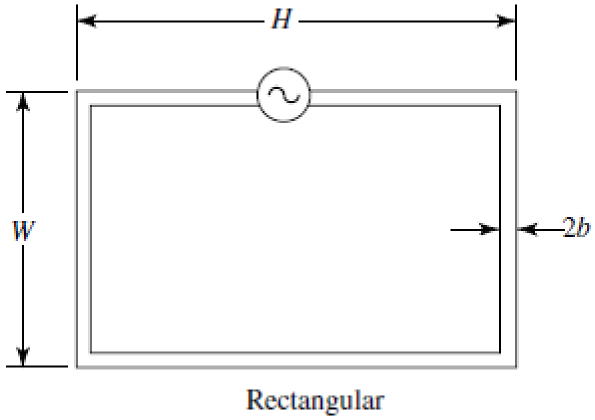

Figure 54 Typical configuration of a rectangular loop antenna [4]

The dimensions of the rectangular loop antenna are 76mm in width and 86mm in height. This antenna is positioned at 10mm from the human-hand-like brick. The loop antenna resonates at 1GHz.

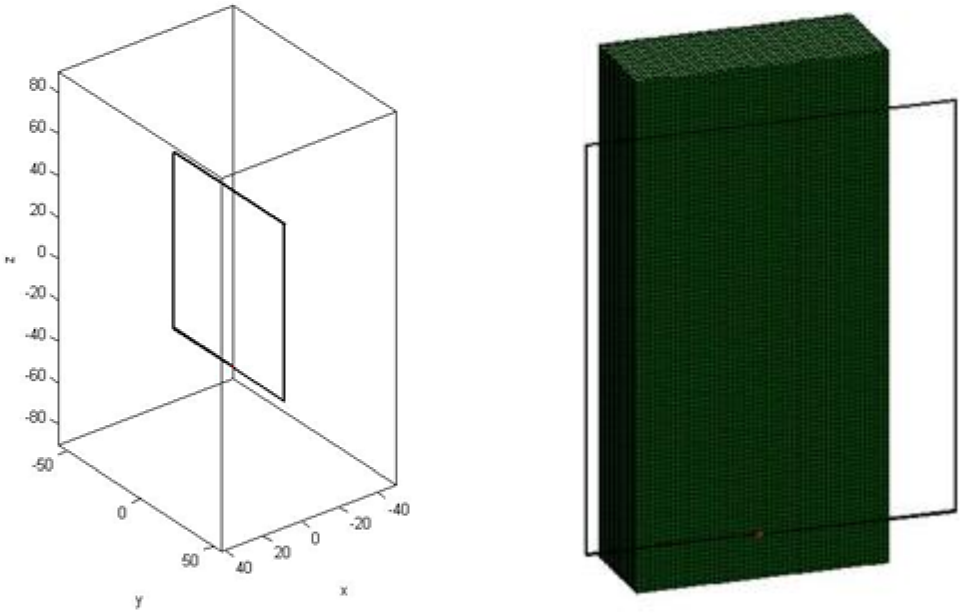

Figure 55 Design of a rectangular loop antenna in free space (left) and facing a human-hand-like dissipative brick (right)

2) Results of the robustness experiment

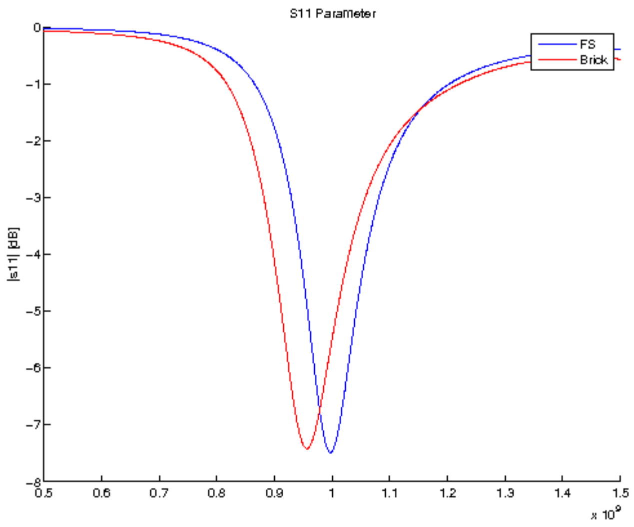

Figure 56 Impact of the human-hand-like brick on the S11 parameter of the loop antenna

When considering the reflection coefficient of the loop antenna, the influence of the human hand can be characterized as such:

The overall value of the reflection coefficient at the resonant frequency does not vary much, and remains constant at a value of -7.5 dB. At the desired frequency of 1GHz, the reflection coefficient of the loop antenna with the brick rises to -5.5dB, making it very vulnerable to interference and thus a poor choice for an antenna. However, the resonant frequency sets to 950MHz instead of the designed 1GHz (50MHz variation). The bandwidth of the loop antenna in free space is 134MHz, and 189MHz with the brick. This represents a 32% variation.

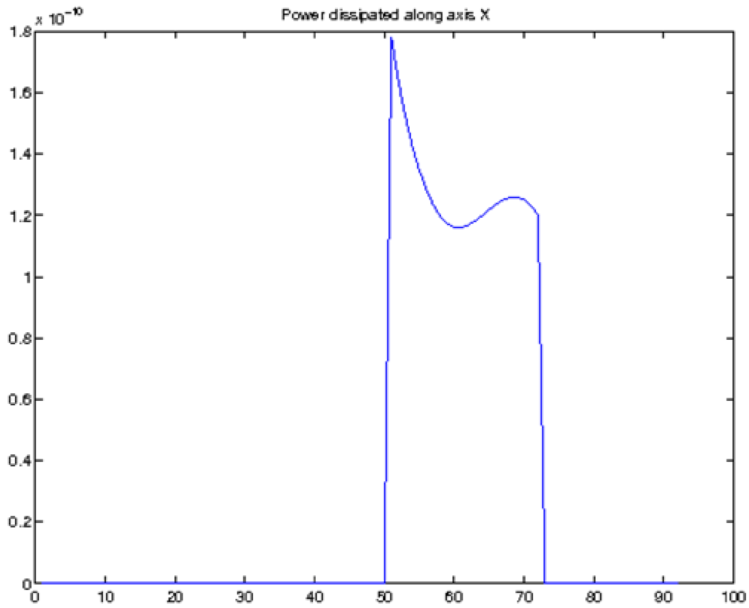

Figure 57 Dissipation (in W) along the radial axis of a loop antenna facing a 22mm-wide human-hand-like brick

Unlike most antennas in this study, the power dissipation within the brick of the loop antenna is smooth. The peak of dissipation, when the fields enter the brick, is at $1.8*10^{-10}$ W and drops to a minimum of $1.15*10^{-10}$ W at the center of the brick before rising again to a value of $1.25*10^{-10}$ W. The spread of these values is minimum compared to other discussed antennas.

The total power dissipated is $2.83*10^{-9}$ W, and the input power of $5.63*10^{-9}$ W, which means 50% of the input power is dissipated within the brick. This is the lowest amount reached within this study. The power dissipated in the first half of the brick is $1.61*10^{-9}$ W (56.7% of the total power dissipated).

The loop antenna has the highest 3D correlation coefficient (0.97), meaning that is one of the most predictable antennas in this study.

3) Conclusion

Overall, the loop antenna is less vulnerable than other antennas in this study with regard of the impact of the hand on its performance. It dissipates one of the smallest amounts of radiated power in the hand between the antennas displayed here. However, the flaw of the loop antenna is that it is not easily implemented on a mobile handset due to the size requirements.

X – Folded loop antenna

1) Presentation

The folded loop antennas act similarly to loop antennas; however the key objective when “folding” a loop antenna is to reduce its size in order to benefit from the advantages of the loop antenna in small-sized systems.

The loop antenna in this study has the following characteristics:

The antenna is 46mm in width, and 40mm in height. On both vertical sides, 15mm from the top and the bottom, a 10mm-high “fold” is inserted, this fold is 20mm-large. This antenna resonates at 0.9GHz.

This folded loop antenna is set on a 46mm-wide and 60mm-high ground plane, modeling the mobile handset.

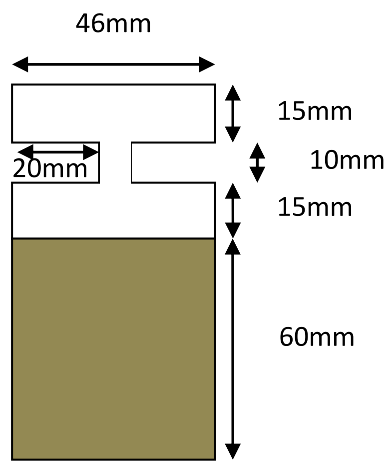

Figure 58 Dimensions of a folded loop antenna

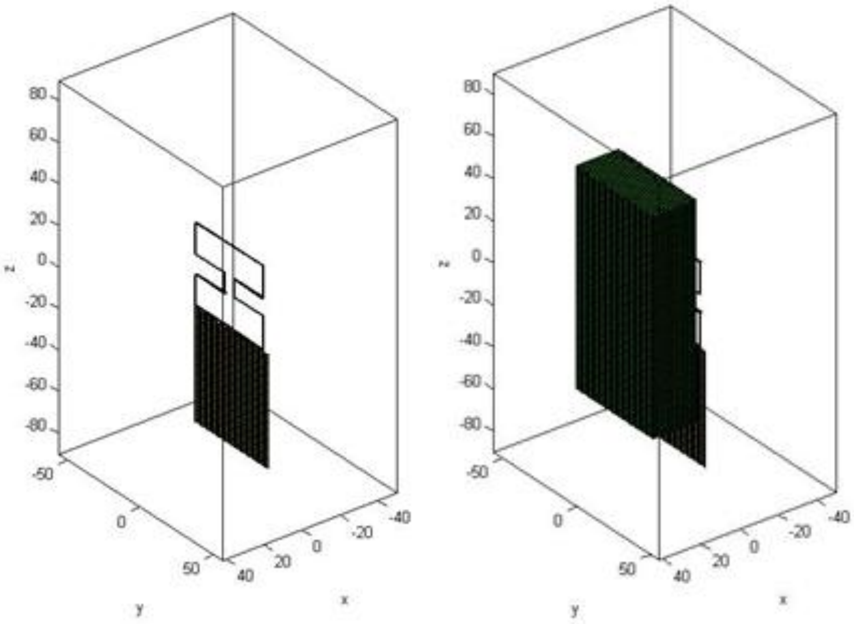

Figure 59 Design of a rectangular folded loop antenna in free space (left) and facing a human-hand-like dissipative brick (right)

2) Results of the robustness experiment

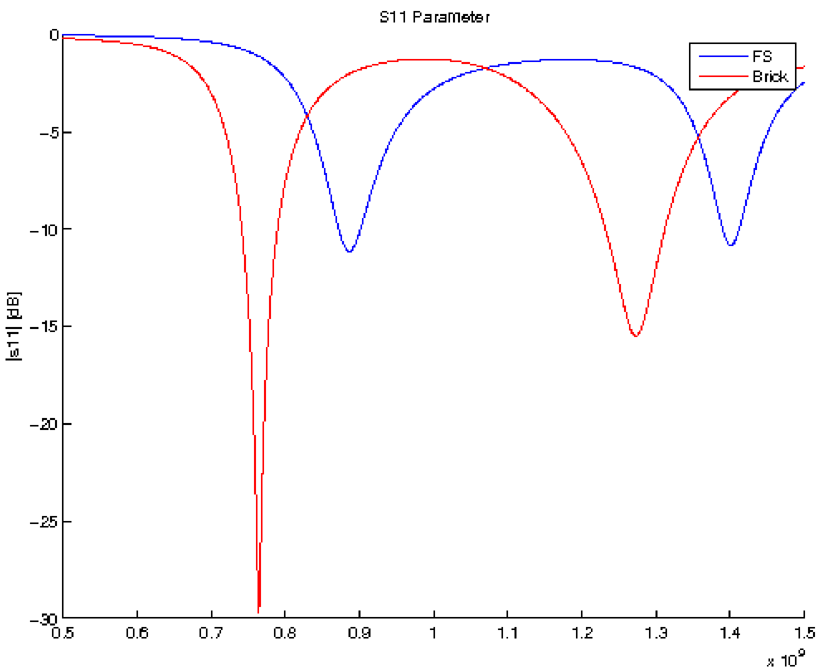

Figure 60 Impact of the human-hand-like brick on the S11 parameter of the folded loop antenna

When considering the reflection coefficient of the folded loop antenna, the influence of the human hand can be characterized as such:

- The value of the reflection coefficient is greatly impacted. As can be seen on the previous figure, its value drops from -11dB (in the free space case) to -30dB (when considering the brick). Thus in a way, the brick makes the antenna more resilient to further interference.
- The bandwidth is 59MHz in free space and 75MHz considering the brick at their respective resonant frequency. This is a 34% variation, analogous to the loop antenna studied above.
- However, the resonant frequency is displaced by 130MHz, from 900MHz to 770MHz. This shift is one of the most important observed in this study.

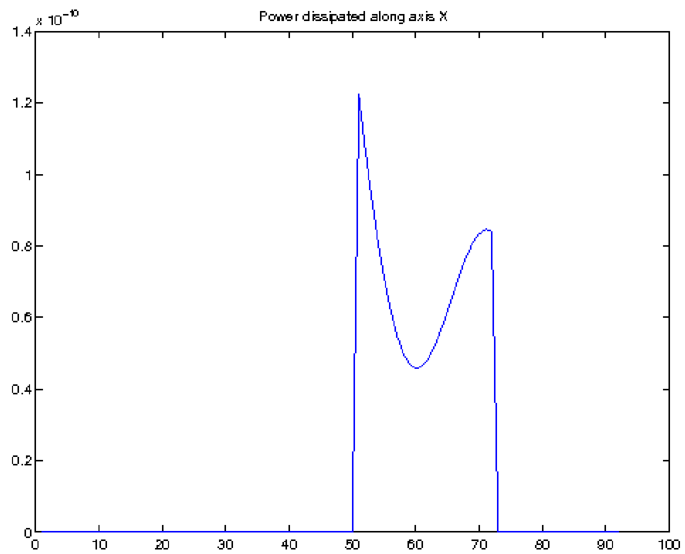

Figure 61 Dissipation (in W) along the radial axis of a folded loop antenna facing a 22mm-wide human-hand-like brick

The behavior of the folded loop antenna power dissipation has the same typical shape as the other antennas. The peak of dissipation, when the fields enter the brick, is at $1.2*10^{-10}$ W and drops to a minimum of $0.50*10^{-10}$ W at the center of the brick before rising again to a value of $0.85*10^{-10}$ W.

The total power dissipated is $1.55*10^{-9}$ W, and the input power of $1.97*10^{-9}$ W, which means 79% of the input power is dissipated within the brick. This is the one of the highest amount reached within this study, making this antenna a poor-value antenna. The power dissipated in the first half of the brick is $8.32*10^{-9}$ W (53.6% of the total power dissipated).

3) Conclusion

The impact of the human hand on the folded loop antenna is both beneficial and damaging. On one hand, the reflection coefficient improves with the presence of the brick, but on the other hand, the shift in resonant frequency is considerable. The folded loop antenna has one of the smallest input power dissipation among the antennas surveyed.

CHAPTER FIVE: PARAMETERISATION AND ROBUSTNESS CRITERION

In this chapter, we will present the results of our different calculations and the antenna ranking in term of robustness established from them.

I – Percentage of power dissipated

Using a Matlab script, we have determined the quantity of power which has been dissipated in the “test brick”. We have then made a ratio of this quantity over the input power to classify the antennas regarding the fact that they lose the less power as possible inside the brick.

Here is a sum-up table of the results:

	Dissipated power (W)	Input Power (W)	Dissipated power (%)
Loop	2,84E-09	5,63E-09	50,38%
PIFA	1,93E-09	3,73E-09	51,63%
PIFA with substrate	1,75E-09	3,33E-09	52,43%
Slotted PIFA	9,25E-10	1,57E-09	58,80%
Dipole	4,83E-09	7,18E-09	67,21%
Monopole	5,21E-09	7,56E-09	68,84%
Narrowband PIFA	1,66E-09	2,29E-09	72,51%
Folded loop	1,55E-09	1,97E-09	78,59%
IFA	4,45E-09	5,09E-09	87,46%

Table 8 Power dissipated for the different antennas

What is really important in this table is the dissipated power in percentage. The less dissipative antenna dissipates 50.38% of its input power against 87.46% for the most dissipative. Only the loop antenna, the PIFA, the PIFA with substrate and the slotted PIFA are under 60% of dissipated power, percentage which seems correct for an antenna according to the data obtained during this survey. Power dissipation is the most important factor when considering robustness.

The dipole and the monopole antenna have similar power dissipated (67.21% and 68.84%). The narrowband PIFA and the folded loop dissipate over than 70% of the input power (72.51% and 78.59%). Finally, the IFA dissipates the major part of its input power (87.46%).

According to this method, the best antenna is the loop antenna. However, due to the size requirements of the loop antenna which cannot, or hardly, be achieved on a mobile handset, the PIFA seems a better choice. Incidentally, today's mobile phones mostly rely on PIFAs. When considering the PIFAs, the best choice seems to be the regular PIFA, followed by the PIFA with substrate and finally the slotted PIFA.

II – 3D Correlation of E-fields

This method consists of a normalized cross correlation in three dimensions between the electric fields of the simulation of the antenna in free space and the electric fields obtained from the simulation of the antenna with the test brick. This way, we measure how much the fields can be predictably altered by the human hand.

The Matlab script is based on the function "normxcorr3" developed by Daniel Eaton, initially made for some medical imaging purposes and which is derived from the Matlab "normxcorr2" function.

The following table sums up the results obtained:

	3D-Correlation
Loop	97,50%
Dipole	93,82%
Narrowband PIFA	93,44%
IFA	89,22%
Monopole	88,78%
Folded loop	85,35%
Slotted PIFA	82,94%
PIFA with substrate	78,21%
PIFA	77,95%

Table 9 3D-correlation coefficients

By considering correlation, it is meant that a high correlation coefficient implies that the electric fields of the antenna with the presence of the hand vary according to the same trends. A lower correlation coefficient means that the variations of the electric fields with the hand are less predictable. Generally the shapes of the electric fields are not so much altered by the brick or are altered according to common trend. Indeed, all the correlations are over 77%, and the best 3D correlation is over 97%, which is really high. The loop antenna has the highest correlation with 97.50%. The dipole antenna and the narrowband PIFA are around 93% (93.82% and 93.44%). THE IFA and the monopole are close with 89.22% and 88.78%. And the most affected antennas are the slotted PIFA (82.94%), the PIFA with substrate (78.21%) and the PIFA (77.95%). Even if there is 20% between the highest and the lowest value of the 3D correlation, it is shown that the shape of electric field is not so much disturbed by the brick.

According to this method, the antenna which produces electric fields the least affected by the brick is the loop antenna.

III – General shape evaluation

In order to classify the antenna based on the graphical representation of the S11 parameters, we firstly decided to make a cross correlation between the data of the s11 obtained in free space and the ones from the s11 obtained with the test brick.

The results we have obtained are listed on the following table:

	Cross-correlation
Slotted PIFA	0,996
Narrowband PIFA	0,987
Monopole	0,978
Folded loop	0,966
Loop	0,947
Dipole	0,658
PIFA	0,521
PIFA with substrate	-0,266
IFA	-0,464

Table 10 Cross-correlation coefficients of S11 curves

The results of cross correlation between the S11 are quite different. Indeed, the best cross-correlation goes until 0.996, but the worst is -0.464. The S11 could be really affected by the brick. The less disturbed by the brick are the slotted PIFA (0.996), the narrowband PIFA (0.987), the monopole antenna (0.978), the folded loop antenna (0.966) and the loop antenna (0.947). All of these antennas have a cross-correlation over 0.9 which shows that the S11 is not too much affected by the brick. But for other antennas, the difference between the both S11 is more important. Indeed, the dipole antenna (0.658), the PIFA (0.521), the PIFA with substrate (-0.266) and the IFA (-0.464) are really affected by the brick.

Unfortunately, these results didn't appear to be of any real value. This is why it was decided to proceed to a visual comparison of the different graphs and then establish a ranking based on the impact on the shape.

For this visual method, the ranking is now as follows (from the best to the worst antenna):

Monopole
Dipole
Loop
Slotted PIFA
IFA
Folded loop
PIFA with substrate
PIFA
Narrowband PIFA

Table 11 Visual ranking

IV – Variation of the resonant frequency and the associated S11 parameter

Firstly, a comparison of the variation of the resonant frequency calculated by the AAU3 software between the free space simulations and the simulations with a brick.

The following table sums up the results:

	Free space freq. (Hz)	Brick freq. (Hz)	Variation (Hz)
Monopole	9,80E+08	9,85E+08	5,00E+06
Dipole	9,94E+08	9,63E+08	3,10E+07
Loop	9,97E+08	9,56E+08	4,10E+07
Narrowband PIFA	1,02E+09	9,63E+08	5,20E+07
IFA	1,02E+09	9,13E+08	1,02E+08
Folded loop	8,86E+08	7,64E+08	1,22E+08
Slotted PIFA	9,93E+08	8,42E+08	1,51E+08
PIFA with substrate	9,85E+08	8,12E+08	1,73E+08
PIFA	1,02E+09	8,38E+08	1,85E+08

Table 12 Resonant frequencies for the different antennas

This table shows important difference between the behaviors of the resonant frequency for each antenna. Indeed, the less disturbed frequency move only from 5MHz, but the most disturbed move from 185MHz which is really noticeable. The monopole antenna has a very low variation of its resonance frequency (5MHz). The resonance frequency is more affected but less than 60MHz for the dipole antenna (30MHz), the loop antenna (41MHz) and the narrowband PIFA (52MHz). But some antennas have their resonance frequency moved more than 100MHz. It’s the case for the IFA (102MHz), the folded loop antenna (122MHz), the slotted PIFA (151MHz), the PIFA with substrate (173MHz) and the PIFA (185MHz).

We have then evaluated the variation of the S11 at the resonant frequency:

	S11 FS (dB)	S11 brick (dB)	Variation (dB)
Loop	-7,49	-7,42	0,07
Dipole	-14,92	-14,00	0,92
Monopole	-12,30	-15,35	3,05
PIFA with substrate	-13,97	-17,07	3,10
PIFA	-10,45	-14,11	3,66
IFA	-17,13	-8,02	9,12
Slotted PIFA	-25,88	-13,37	12,51
Folded loop	-11,14	-29,69	18,55
Narrowband PIFA	-25,37	-3,44	21,93

Table 13 S11 variations

It is interesting to see that the S11 at the resonance frequency could vary from only 0.07dB to 21.93dB, depending on the antenna, which is a difference of 300% between the most and the less affected antenna. The S11 at the resonance frequency is not affected for the loop antenna (0.07dB) and few affected for the dipole antenna (0.92dB). Around a variation of 3dB, there are three antennas, the monopole antenna (3.05dB), the PIFA with substrate (3.10dB) and the PIFA (3.66dB). The other antennas have a variation from 3 to 7 times more important. Indeed, the variations of the S11 at the resonance frequency are really important for the IFA (9.12dB), the slotted PIFA (12.51dB), the folded loop antenna (18.55dB) and the narrowband PIFA (21.93).

The loop antenna is the antenna which his having the smallest variation of the s11.

V – Evolution of the Efficiency

Here are the results compiled from AU3 and showing the evolution of the efficiency in case of a free space simulation or with the brick. The antennas have been ranked according to the variation of this efficiency (the smaller, the better):

	Efficiency FS	Efficiency brick	Variation
Loop	0,9228	0,4579	50,38%
PIFA	0,9940	0,4834	51,37%
PIFA with substrate	0,9597	0,4610	51,96%
Slotted PIFA	0,9866	0,3974	59,71%
Dipole	0,9866	0,3293	66,62%
Monopole	0,9876	0,3122	68,39%
Narrowband PIFA	0,9933	0,2721	72,61%
Folded loop	0,9966	0,2135	78,58%
IFA	0,9992	0,1246	87,53%

Table 14 Antennas efficiencies

This table shows that the efficiency varies at least from 50% with the presence of the brick. Despite these high variations there are some antennas less affected than others. Indeed, there are 4 antennas which have a variation less than 60%, the loop antenna (50.38%), the PIFA (51.37%), the PIFA with substrate (51.96%) and the slotted PIFA (59.71%). Two other antennas have a variation between 60 and 70%, the dipole antenna (66.62%) and the monopole antenna (68.39%). And the other antennas have a variation over 70%, the narrowband PIFA (72.61%), the folded loop antenna (78.58%) and the IFA (87.53%), which has its efficiency greatly reduced.

As seen in the previous table, and for this criterion, the loop antenna is the most robust one.

VI – Global view of the rankings

The following table is summing up the rankings of the antennas according to the methods we used previously.

	Power dissipated	3D correlation	Visual	Resonant freq.	S11	Efficiency
Loop	1	1	3	3	1	1
Dipole	5	2	2	2	2	5
Monopole	6	5	1	1	4	6
Slotted PIFA	4	7	4	7	6	4
PIFA with substrate	3	8	7	8	3	3
PIFA	2	9	8	9	5	2
Narrowband PIFA	7	3	9	4	8	7
IFA	9	4	5	5	7	9
Folded loop	8	6	6	6	9	8

Table 15 Antennas final rankings

This table shows the difficulty of finding one really particularly robust antenna compared to the others. The ranking shows that depending on the criteria, there are different antennas ranked first. But with the averaging of the ranking for each criterion, it is shown that the loop antenna has the best overall ranking. However, the loop antenna is not easily implemented on a mobile phone.

CONCLUSION

At the beginning of this project, it was clearly known that there was little if not almost no theory concerning the topic chosen and thin leads on the proper way to follow. The aim of this project was to be a survey that would later lead on further research on the topic.

The main objective of this thesis was to find a brick to define properly the human hand and a criterion for the robustness of antennas. Defining the brick has come to be a success, allowing future research to simulate the hand with an easier model to simulate the interactions of the antenna with it. However, there was never just one, but a great number of criterions for the robustness. According to the main focus of the antenna (the S11, the efficiency, the power dissipated…), the most robust antenna changed.

In the end, while the results obtained display several trends in the variation of the performance of an antenna when placed near a human hand (variation of the reflection coefficient, variation of the bandwidth, power dissipation), there is not one and only robust antenna according to the tools used in this survey.

Therefore, there are two leads to continue this research; either define a new set of tools based on the results obtained in this survey and the general trends they show; or it might just be that the robustness of an antenna is just like the design of a new antenna : it can only be based on empirical observations and thus cannot be theorized.

APPENDIX

Smith Chart

The Smith chart is a basic method for determining circuit fundamentals. It is usually used to represent parameters like impedances, admittances, scattering parameters and reflection coefficients and permits to solve problems with transmission lines and matching circuits.

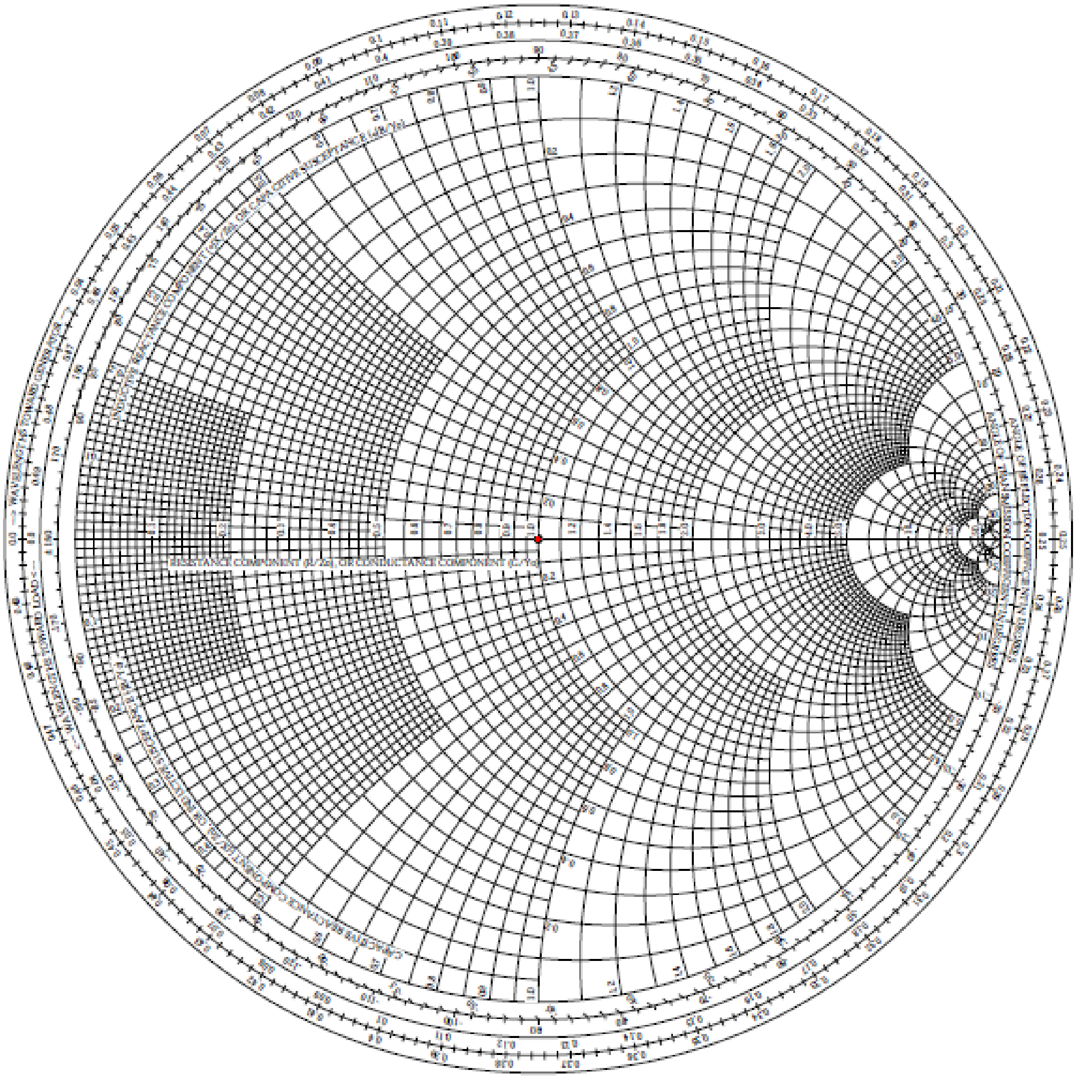

Figure 62 Smith Chart

Any impedance, Z= R+jX, can be represented on the Smith Chart.

The position of this impedance is located at the intersection of the constant resistance and reactance circles that we consider.

Each circle, in the smith chart is representing a constant resistance [8], as we can see on the next scheme. The real part of the impedance is then used to determine on which constant resistance circle the impedance is represented[12].

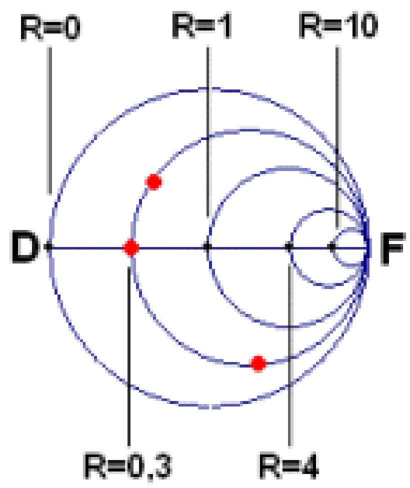

Figure 63 Impedance circles

Each red point, on the scheme, has the same resistance (R=0.3), but they do not have the same reactance [13].

The line between the point D and the point F represent all the impedances with an imaginary part equal to zero.

The point D represents an impedance equal to zero (short circuit). The point F represents an impedance with an infinite imaginary part (open line).

The imaginary part is used to determine on which constant reactance circle the impedance will be represented.

These constant reactance circles are represented on the next scheme:

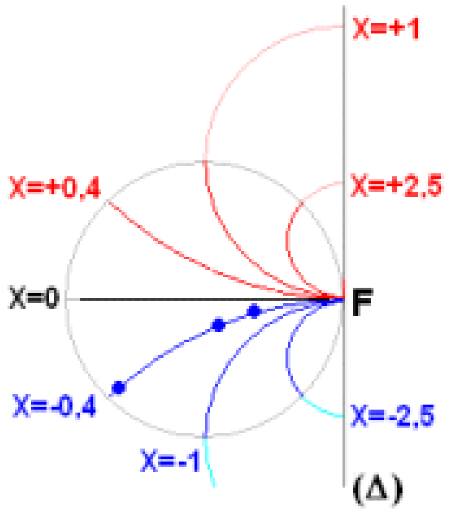

Figure 64 Imaginary parts

Each blue points, on the previous scheme, has the same reactance (X=-0.4), but they don't have the same real part.

All the inductive reactance (X>0) are in red on the previous scheme, and the capacitive reactance (X<0) are in blue.

On the next scheme, which is a normalized Smith Chart[11], the green circle is representing all the impedances Z=1+jX, X being real.

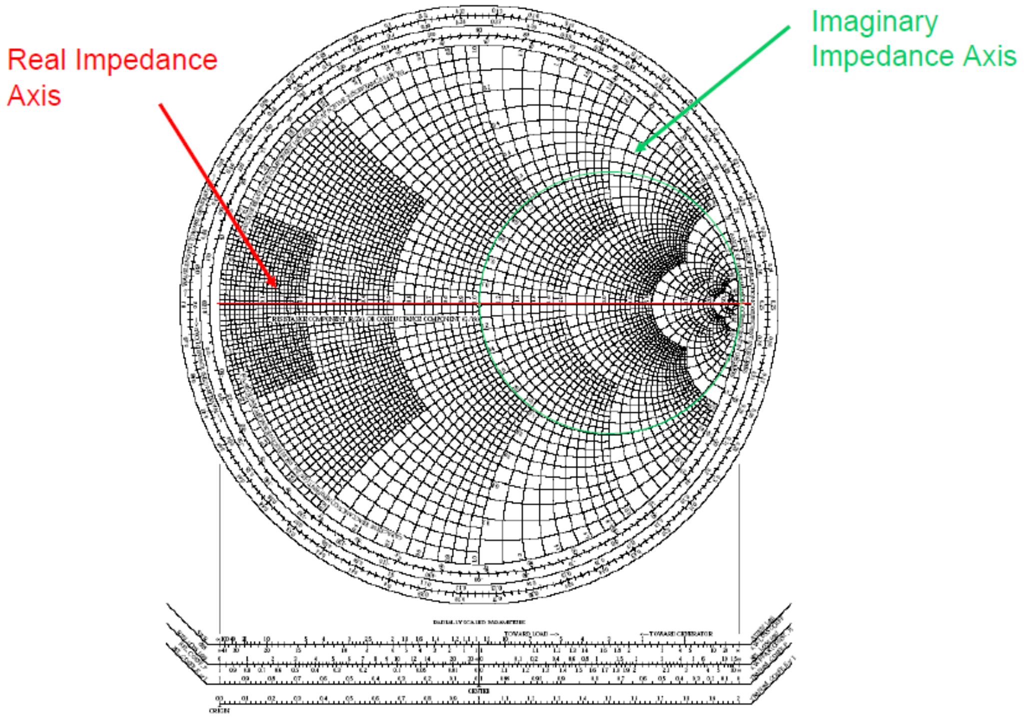

Figure 65 Impedance axes

With this normalized Smith Chart, each part of the impedance must be divided by the characteristic impedance Z0 of the transmission line. The representation uses the normalized impedance.

For example, the representation of the normalized impedance Z=0.3+0.4j, is on the next graph:

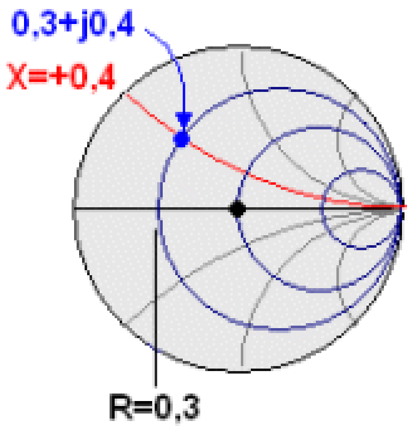

Figure 66 Total impedance

The reflection coefficient is $\Gamma = \frac{Z - Z_0}{Z + Z_0}$ with Z_0 the characteristic impedance can be read on the Smith Chart. It's given by the line between the point representing the impedance, and the center of the Smith chart (R=1 and X=0). Indeed, the smith chart is the representation of the reflection coefficient in polar coordinates.

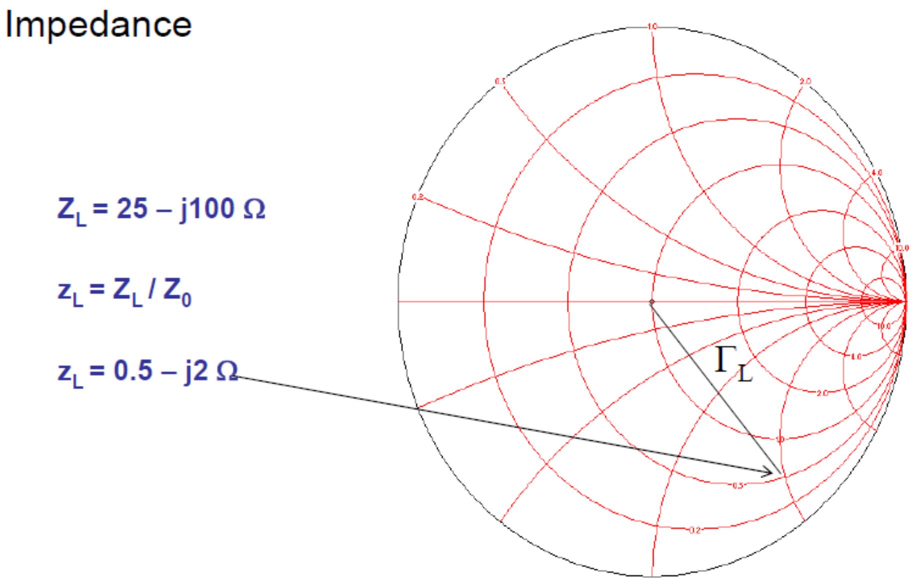

Figure 67 Reflection coefficient at the transmission line

The scale around the smith chart represents the wavelength but also the angle of the reflection coefficient:

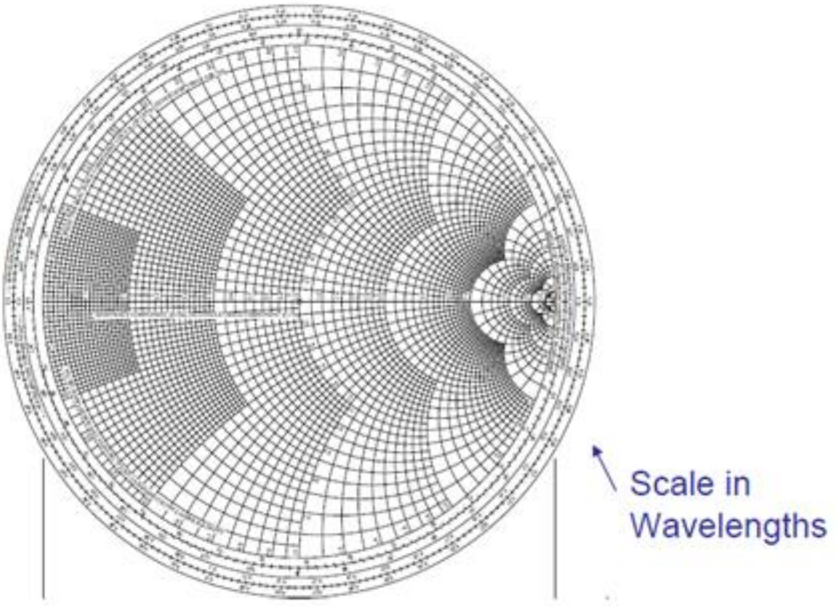

Figure 68 Wavelength scale

So, we are able, thanks to the Smith chart, to have the reflection coefficient in function of frequency.

REFERENCES

[1]http://money.cnn.com/galleries/2010/technology/1007/gallery.iphone_problems/index.html

[2] User's Influence Mitigation for Small Terminal Antenna Systems, Mauro Pelosi

[3] Computationnal Electrodynamics: The Finite Difference Time Domain Method, Allen Taflove

[4] Antenna Theory Analysis and Design, Constantine A. Balanis

[5] http://mathbits.com/mathbits/tisection/statistics2/correlation.htm

[6] http://www.experiment-resources.com/pearson-product-moment-correlation.html

[7] Les Antennes : Théories, conceptions et applications, Odile Picon

[8] http://www.antenna-theory.com/basics/impedance.php

[9] http://www.antenna-theory.com/antennas/smallLoop.php

[10] http://www.allenhollister.com/allen/files/scatteringparameters.pdf

[11] Lectures on microwaves Part 4- Smith Chart, Xavier Le Polozec, ECE Paris 2010

[12] http://www.antenna-theory.com/tutorial/smith/chart.php#smithchart

[13] http://f5zv.pagesperso-orange.fr/RADIO/RM/RM23/RM23p/RM23p01.html

[14] Interaction between mobile terminal antenna and user, Juho Poutanen

[15] On the general energy absorption mechanism in the human tissue, Outi Kivakäs, Tuukka Lehtiniemi, Pertti Vainikainen

[16] AAU3 User Manual

[17] http://www.antenna-theory.com/antennas/halfwave.php

[18] http://www.antenna-theory.com/antennas/monopole.php

[19] http://www.ahsystems.com/catalog/SAS-563B.php

[20] http://www.supernec.com/ifa.htm

[21] Kin-Lu Wong, Dept. Of Electrical Engineering, National Sun Yat-Sen University

[22] http://www.antenna-theory.com/antennas/patches/pifa.php